Spring 1-1-2016

# Coupling Fluvial-Hydraulic Models to Study the Effects of Vegetation on Sediment Transport and Flow Dynamics in the South Platte River, Colorado

Garrett William Sprouse
*University of Colorado at Boulder*, garrett.sprouse@colorado.edu

# COUPLING FLUVIAL-HYDRAULIC MODELS TO STUDY THE EFFECTS OF VEGETATION ON SEDIMENT TRANSPORT AND FLOW DYNAMICS IN THE SOUTH PLATTE RIVER, COLORADO

by

GARRETT WILLIAM SPROUSE

B.S., University of Colorado, 2014

A thesis submitted to the

Faculty of the Graduate School of the

University of Colorado in partial fulfillment

of the requirement for the degree of

Master of Science

Department of Civil, Environmental, and Architectural Engineering

2016

This thesis entitled:

Coupling Fluvial-Hydraulic Models to Study the Effects of Vegetation on Sediment Transport and Flow Dynamics in the South Platte River, Colorado

written by Garrett William Sprouse

has been approved for the Department of Civil, Environmental, and Architectural Engineering

_____

John Pitlick

_____

Roseanna Neupauer

_____

Hari Rajaram

Date_____

The final copy of this thesis has been examined by the signatories, and we find that both the content and the form meet acceptable presentation standards of scholarly work in the above mentioned discipline.

# Abstract

Sprouse, Garrett William (M.S., Civil Engineering)

Coupling Fluvial-Hydraulic Models to Study the Effects of Vegetation on Sediment Transport and Flow Dynamics on the South Platte River, Colorado

Thesis directed by Professor John Pitlick

This study investigated the effects of riparian vegetation on sediment transport rates and flow dynamics in the South Platte River just downstream of Fort Lupton, Colorado. FaSTMECH, a two-dimensional coupled fluvial and hydraulic model, was used to compute flow characteristics (velocity and depth) in addition to sediment mobility characteristics (shear stress and sediment flux) for four discharge levels ranging from 5% of bankfull flow to bankfull flow ($Q_{bf}$). Estimates of a dimensionless drag coefficient ($C_d$) representative of the middle-aged bushy willows found on the river banks at the study site were used to create a spatially variable roughness in the model throughout the river reach. Model results show that during average annual flood events, vegetation on the river banks causes increased drag forces on the flow, leading to an increased proportion of flow being diverted into the main channel and resulting in higher velocities. The spatial distribution of shear stresses collapse under these conditions with an order of magnitude decreases over river banks and significant increases throughout the main channel. Sediment fluxes in the reach increase by nearly an order of magnitude with the presence of bank vegetation, however, the greatest differences occur during $Q_{bf}$ when the highest fraction of the sediment is mobile. Further analysis of vegetation effects was conducted by performing a sensitivity analysis by altering the representative non-dimensional vegetation drag coefficient by

as much as +/- 400%. These alterations represent differences in vegetation density, height, orientation, leafy/leafless structure, age, rigidity, and vegetation type. Although there is a relationship between sediment fluxes and changes in $C_d$, there only exists a 14% increase in transport at $Q_{bf}$ between the two exterior limits of $C_d$.

*To my father who showed me a passion for science and*

*a love for the great outdoors.*

*To my mother who has always supported me and encouraged*

*me along every step of the way.*

# Acknowledgements

First and foremost I would like to thank my advisor John Pitlick for his continued support and mentorship. John has always been very willing to help me with my studies and my research. When I first went to John, I only had a broad idea of what I wanted to do, but he helped turn my passion for knowledge and the outdoors into an amazing thesis. I truly appreciate how willing John always was to go out in the field with me to get measurements. It didn't matter if it was wet and muddy or blisteringly hot and humid, John was always there to help. My knowledge in the field of hydrology and geomorphology has immensely increased thanks to him. John has been more than just an advisor and a mentor, he has been a great friend.

I would also like to thank my other committee members, Roseanna Neupauer and Hari Rajaram. Both individuals have been great influences in my graduate career and both have taken the time to sit down with me and help me find a fitting research path. I have learned a great deal from the two of them, both inside the classroom and out.

Many people know that modeling can be a difficult and sometimes very frustrating process, especially when using a new model that you are unfamiliar with. Thankfully, Rich McDonald helped provide guidance throughout the entire process. Rich was an amazing resource to have. He not only helped ensure my simulations were running correctly and helped provide me with tips to make the process run much more smoothly and quickly, but he is also a very enjoyable person to grab a cup of coffee with.

I have had a lot of fun with this project, especially my times out in the field. John and I worked through rain, snow, and shine, battled through dense vegetation, fell into rivers, went on some great hikes, and rafted down the not so roaring South Platte River. It has been a great

experience, filled with both laughter and fun as well as a great deal of learning and knowledge gathering. I must extended a special thank you to Bill Lewis for allowing me to have all these experiences. Bill is the owner of the land we worked on and was nothing less than a true gentleman and scholar. Bill gave John and myself free reign and access to his property so we could work at times convenient for us and during flow events of particular interest.

Lastly, I would like to thank my friends and family, for which none of this would have been possible without. My mom and dad, Karen and Bill, have always encouraged and supported me in everything I do. I am truly lucky to call them my parents and am incredibly grateful to have their backing. To all my friends back home, thank you for helping show me the wonder of the world and for going on adventures in the mountains with me. For all my friends in Boulder, thank you for an amazing college experience. To all of you, I am deeply grateful.

# Table of Contents

# List of Figures

# List of Tables

# List of Symbols

| Symbol | Units | Definition |
|---|---|---|
| $A_{relax}$ | [-] | Adjustment for the global shape of WSE at each iteration |
| B | [L] | Water surface width |
| $C_d$ | [-] | Dimensionless drag coefficient |
| $C_{d\text{-}channel}$ | [-] | Dimensionless drag coefficient for the river channel |
| $C_{d\text{-}floodplain}$ | [-] | Dimensionless drag coefficient for the floodplain |
| $C_{d\text{-}veg}$ | [-] | Dimensionless drag coefficient of vegetation |
| $C_{d,veg\text{-}channel}$ | [-] | Dimensionless drag coefficient for vegetation in the channel |
| $C_{d,veg\text{-}floodplain}$ | [-] | Dimensionless drag coefficient for vegetation on the floodplain and banks |
| $d_{84}$ | [L] | $84^{th}$ percentile particle diameter |
| D | [L] | Particle grain dimeter |
| $D_{50}$ | [L] | $50^{th}$ percentile particle diameter |
| $D^*$ | [-] | Dimensionless grain size |
| $E_{relax}$ | [-] | Relaxation coefficient for the WSE |
| f | [-] | Friction factor |
| g | $[L/T^2]$ | Gravitational constant |
| h | [L] | Flow deptj |
| $\bar{h}$ | [L] | Mean flow depth |
| $\overline{h_{bf}}$ | [L] | Average bankfull depth |
| k | [-] | Von Karman's constant (typically = 0.4) |
| LEV | $[L^2/T]$ | Lateral eddy viscosity |
| n | [-] | Manning's roughness coefficient |
| $n_{floodplain}$ | [-] | Adjusted Manning's n representing the vegetated surface |
| $q_T$ | $[L^2/T]$ | Total sediment flux per unit width ($Q_T/B$) |
| Q | $[L^3/T]$ | Discharge |
| $Q_B$ | $[L^3/T]$ | Flux of bed load |
| $Q_{bf}$ | $[L^3/T]$ | Bankfull discharge |
| $Q_S$ | $[L^3/T]$ | Flux of suspended load |
| $Q_{sed}$ | [M/T] | Sediment flux |
| $Q_T$ | $[L^3/T]$ | Total sediment flux (= $Q_B + Q_S$) |
| R | [-] | Submerged specific gravity (1.65 for quartz) |
| RMSE | [L] | Root mean squared error |
| s | [-] | Specific gravity of sediment (2.65 for quartz) |
| S | [L/L] | Reach slope |

| | | |
|---|---|---|
| u | [L/T] | Velocity in down-stream direction |
| $\bar{U}$ | [L/T] | Mean flow velocity |
| $U_{relax}$ | [-] | Relaxation coefficient for velocity |
| v | [L/T] | Velocity in cross-stream direction |
| WSE | [L] | Water surface elevation |
| $y_i$ | [L] | Observed value for the $i^{th}$ observation |
| $\hat{y}_i$ | [L] | Predicted value for the $i^{th}$ observation |
| $z_o$ | [L] | Roughness height |
| $\rho$ | [M/L$^3$] | Density of water |
| $\rho_s$ | [M/L$^3$] | Density of sediment (2650 for quartz) |
| $\Phi$ | [-] | Non-dimensional sediment flux |
| $\tau_o$ | [F/L$^2$] | Boundary or bed shear stress |
| $\tau_s$ | [F/L$^2$] | Grain shear stress |
| $\tau_{sd}$ | [F/L$^2$] | Standard deviation of the shear stress distribution |
| $\tau_x$ | [F/L$^2$] | Shear stress in the down-stream direction |
| $\tau_y$ | [F/L$^2$] | Shear stress in the cross-stream direction |
| $\tau^*$ | [-] | Dimensionless shear stress |
| $\tau^*_{bf}$ | [-] | Bankfull dimensionless Shield's number |
| $\tau^*_{bf\_threshold}$ | [-] | Bankfull dimensionless Shield's number at start of "mostly suspension" transport |
| $\nu$ | [L$^2$/T] | Kinematic viscosity of water |
| $\Delta$ | [L] | Bedform wave height |
| $\lambda$ | [L] | Bedform wavelength |

# 1 INTRODUCTION AND OVERVIEW

Riparian vegetation along natural channels often has large effects on the flow characteristics and sediment transport rates of rivers during large flow events. In low sloping sand and gravel-bed rivers characteristic of semi-frequent inundated floodplains, it is often difficult to obtain accurate estimates of sediment transport due to a wide variety of uncertainty in channel characteristics such as bed and energy slope, bed and vegetative roughness, flow depths, channel width, local velocities, grain size distribution, etc. (Clayton and Pitlick, 2007). Assessment of localized sediment transport rates becomes increasingly difficult due to rivers simultaneously having locations within the channel where the bed is essentially immobile while other areas actively entrain bed material. Many transport equations have been created to date, each putting higher priority on different interactions of channel characteristics and the separation of transport into bed load, suspended load, or total load (Molinas and Wu, 2001; van Rijn, 1984a). However, distributions of shear stresses actively control the movement of bed material and often increase with larger discharges (Pitlick and Wilcock, 2001). The immediate response of vegetation along a river tends to be increased sediment transport rates due to larger magnitude shear stress values caused by increases in drag experienced on the bed material.

In recent years, unprecedented environmental and biological concerns have prompted the need for a better understanding of transport mechanisms under natural conditions, motivating several laboratory, field, and numerical studies with the goal of developing new tools to better estimate sediment transport in rivers (López and García, 1998). The past 20 years have fostered significant advances in multi-dimensional hydrodynamic models, making it possible to simulate the interactions of fluid forces and sediment transport in high detail, both at a localized and a

regional scale. Many two and three dimensional (2D and 3D) models, mostly focusing on patterns of shear stress within a river channel, have been used to study sediment transport related to many relevant fields. Studies have been conducted to research variations in bed mobility and shear stresses in single-thread channels (Berenbrock, 2008; Clayton and Pitlick, 2007; Lisle et al., 2000; Nelson et al., 2010; Segura and Pitlick, 2015), topographical influences of meander bend flow patterns (Legleiter et al., 2011; Nelson and Smith, 1989), the spatial and temporal variations on critical habitats of freshwater fish species (Barton et al., 2005) and benthic organisms (Segura et al., 2011), and the evaluation of channel restoration design (Logan et al., 2011). Few have actually studied the effects of riparian vegetation on flow regimes and sediment transport rates on a reach scale, and the studies that have been conducted generally use a numerical modeling approach rather than a multi-dimensional flow model (López and García, 1998; Murray and Paola, 2003; Wu et al., 2005).

Although multi-dimensional hydrodynamic models have advanced significantly in the past few decades, there still exists many challenges in coupling flow and transport models. Channels with time-varying boundary conditions, mobile bedforms, slopes in the streamwise and transverse direction, wide ranges of sediment grain sizes, and spatially variable bed roughness all complicate the calculation process. Additionally, few programs incorporate options to model in-channel or riverbank vegetation, making it more difficult to acquire accurate estimates of the fluvial processes occurring along low sloping vegetated rivers. Because it is often difficult to quantify the contributions of various sources of roughness, a single parameter such as Manning's n or a drag coefficient is used to lump all the sources of roughness into a common term (Logan et al., 2011). Other models partition the total boundary shear stress into three components: (i) a skin friction bottom stress, (ii) a boundary shear stress equivalent to the dune or ripple form drag, (iii)

and a topographical form drag (Nelson and Smith, 1989). Both methods help to better predict the drag forces associated with riparian vegetation at the bed surface, however, they lack the ability to model the rigid or flexible behaviors of the vegetation above the bed.

The focus of this thesis is to quantify the effects of riparian vegetation on sediment transport rates and flow dynamics on a reach of the South Platte River in Colorado. At the study site, it was observed that the primary vegetation covering the river banks were willow shrubs. The willow ranged in height between 1-2 meters, occupied a moderate to dense vegetation density, and had a leafy structure during the warm and humid months. The FaSTMECH model has the ability to treat bed roughness and vegetation roughness separately for calculation purposes. This led to the need for developing a method for determining a drag coefficient representative of the vegetation found at the study site.

Within the last decade, there have been many studies conducted to determine variable forms of a roughness coefficient for riparian vegetation. These studies vary greatly in their methods and techniques. Numerous studies have utilized the use of small scale flumes to investigate the effects of vegetation density (Chang et al., 2011; Fischenich and Dudley, 2000; Hui et al., 2010; Kim and Stoesser, 2011; Tal et al., 2004; Tanaka and Yagisawa, 2010; Tang et al., 2014), variable vegetation type (Fischenich and Dudley, 2000; Hui et al., 2010; Järvelä, 2002; Tang et al., 2014), and the rigid/flexible nature of vegetation on flow dynamics (Fathi-Maghadam and Kouwen, 1997; Järvelä, 2002; Kim and Stoesser, 2011; Tang et al., 2014). There have also been numerous studies conducted without the use of flumes, focusing more closely on the analytical solutions to flow and the effects of submerged/emergent vegetation (Galema, 2009; Huthoff et al., 2007; Shucksmith et al., 2010). Others utilized numerical models to formulate universal equations for estimating drag coefficients (Hu et al., 2012). Although all

these studies focus on the interaction of vegetation and flow dynamics, there is great variability in the assumptions used. Differences in analytical models, slope of channel, depth of flow, density, size, species type, and orientation of vegetation, and additional parameters all make it difficult to choose a method that closely correlates to the physical situation experienced at the study site.

Throughout the Rocky Mountains of North America, willow communities have dominated the mid-elevation riparian areas. They are largely affected by the magnitude and frequency of large flow events. In order for continuous establishment of point bar willows on meandering rivers, the optimal high flow return period is between 2-5 years (Cooper et al., 2006). The bankfull flow chosen for this study represents the 2 year recurrence interval event, directly aligning with the findings of Cooper et al., 2006. We show that the sediment transport rates in the river reach are orders or magnitude greater for large flow events when riparian vegetation exists compared to a scenario where no vegetation is present.

## Research Objectives:

1. Develop a physically based model incorporating flow dynamics and fluvial processes with both varying discharges and spatially variable roughness at the study site.
2. Compare characteristics of mean normalized shear stress distributions of varying flow and roughness scenarios.
3. Determine differences in sediment loads due to changes in bank roughness caused by the implementation of riparian vegetation.

4. Conduct a sensitivity analysis to compare how changes in bank roughness, controlled by vegetation characteristics, affect sediment transport rates.

# 2 STUDY AREA

The present study focuses on a 0.4 km reach of the South Platte River located just north of Ft. Lupton, Colorado (Fig. 1).

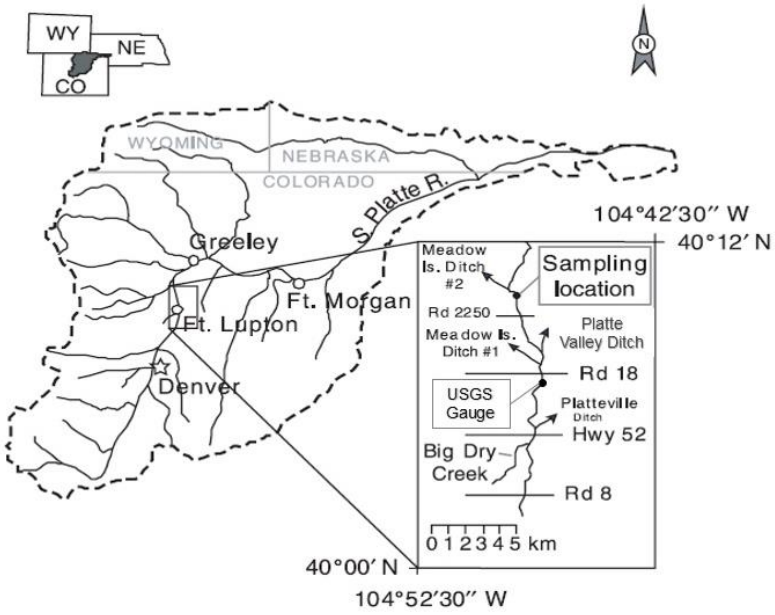


Figure 1. Map of the South Platte River basin showing the study area just downstream (north) of Fort Lupton, CO. This map is a slightly modified version of that shown in Cronin et al., (2007).

This site was chosen because it is mildly sinuous, the channel is self-formed, and the bed consists of large mobile sandbars (Fig. 2).

Figure 2. A photograph of the study site taken from the left (southern) bank looking upstream. It is clear to see the large sandbar in the upper left potion of the photo.

Along the streamwise centerline of the chosen reach, the average slope of the river is approximately 0.001 m/m. Floodplain areas are covered with dense willow between 1-2 meters in height.

The study reach is ideal for studying the effect of vegetation on flow because willow is often the dominant woody plant of riparian zones in montane regions of the western United States (Cooper et al., 2006). This setting provides a unique opportunity to model the effects of vegetation on sediment transport rates in low-sloping rivers, where this specific vegetation type can become established on large sandbars.

The presence of mobile sand bars within the reach provides an additional opportunity to study morphological responses to sediment-transporting flows. The main channel and adjacent banks are comprised of mostly sand-sized sediment that is mobile over a relatively wide range of flows. This makes for large sediment fluxes during high flow events. Figure 3 below shows four aerial images of the study area during different years.


Figure 3. Aerial images showing the variation of location and size of sandbars throughout the study area over a 9-year period.

One feature visible in each photo is a large sandbar on the north bank, which has remained in a nearly constant location over time. Elsewhere, there is considerable variation in the location and size of smaller in-channel sandbars near the upstream and downstream boundaries. The shifting positions of these smaller bars indicates that sediment is transported frequently in this reach. As part of this study, simulations will be run to quantify the effects of vegetation establishment on the large sand bar on sediment transport rates.

# 3 METHODS

## 3.1 Topographical Surveys

The topography of the study reach was measured by surveying a series of 16 cross-sections, encompassing the study reach (Fig. 4).

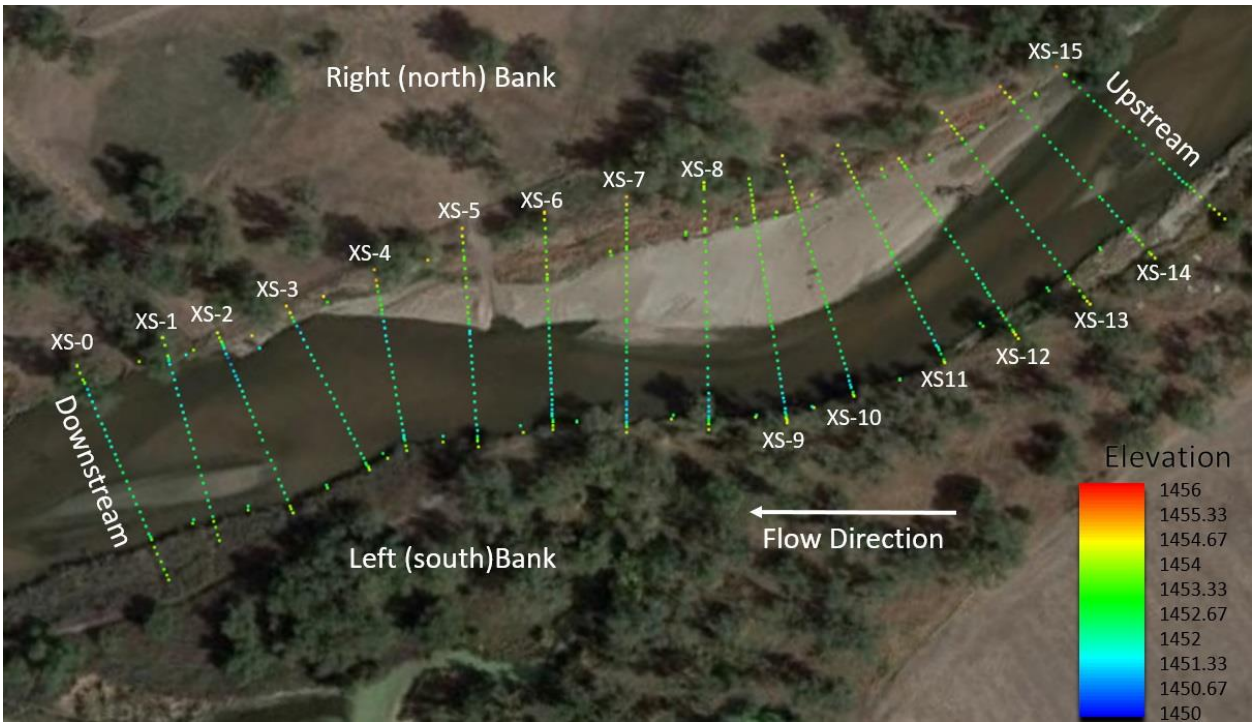


Figure 4. Elevations (in meters above sea level) of all surveyed data points in the study area, clearly showing the orientation and limits of each cross-section.

The spacing between cross-sections was chosen to be approximately half the width of the channel (~25 m). Each cross-section was oriented nearly perpendicular to flow and extended well past the banks onto the adjacent floodplain. Cross-sections were surveyed with a total station, which reads slopes and distances from the instrument to a target location (Fig. 5). Measurements were recorded every 1-2 meters across the channel.

Figure 5. The setup of the total station to get distance and angle measurements of varying locations. In the background of the photo is the large sand bar as well as a dense population of willow bushes.

For this study, we chose the left end point (LEP) of XS-7 to be the local origin (0,0). Every shot taken while using the total station was converted into this local coordinate system using basic geometry.

The elevations of each cross-section end point were established using a Trimble Geo 7X handheld receiver in combination with a Trimble Zephyr Model 2 antenna. This setup uses a dual-frequency (GPS and GLONASS) antenna to minimize errors in low elevation satellite tracking. Elevation results are usually accurate to within a few centimeters.

Once the elevations of the endpoints were established, the elevations of all other intermediate points were calculated based on their relative distance and angle from the corresponding endpoints. Measurements of edges of active channel and tops of banks were taken in between each cross-section on either side of the reach to help the model interpolate elevations in between cross-sections. Finally, water surface elevations were recorded at each cross section

at three separate flow levels. These measurements were used in calibrating the model and are discussed in later sections.

## 3.2 Sediment Data

Sediment was collected in 2006 a few miles upstream of the study area near Fort Lupton, CO. For this study, it was assumed that the distribution of sediment grain sizes has not changed over time or short distances. The median grain size, $D_{50}$, in this section of the South Platte River is 2.7 mm (0.0027 m). Figure 6 below shows the full grain size distribution of the channel bed sediment.

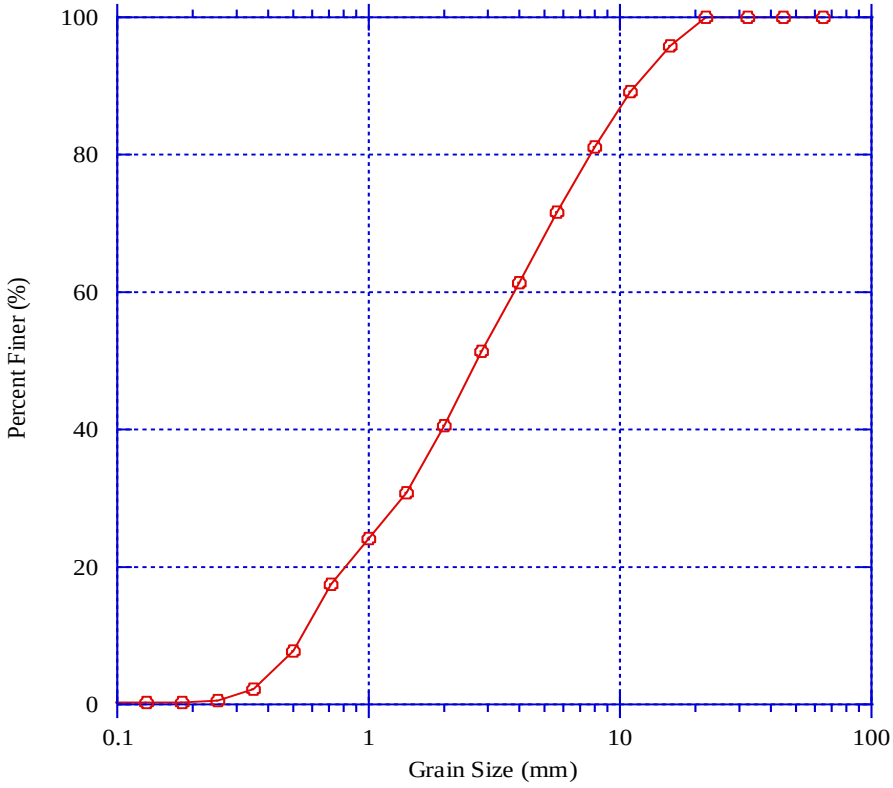


Figure 6. Sediment grain size distribution of the bed material of the South Platte River near Fort Lupton, CO.

## 3.3 Hydrology & Flow Frequency Analysis

The discharge of the South Platte River is measured at a gauging station located about 6.5 km upstream (south) of the study area. The USGS has operated this gauge (No. 06721000) since 1929, however, the record is discontinuous between 1958 and 2002. Between the gauge and the study site, there are two agricultural diversions (Platte Valley Ditch and Meadow Island Ditch No. 1). Both diversions are monitored in a cooperative program between the CDWR, NCWCD, and LSPWCD. In order to estimate the actual discharge at the study site during the times of interest, both diversion discharges were subtracted from the discharges recorded at the upstream USGS gauge.

In addition to diversions for irrigation, the hydrology of the South Platte River has been altered substantially due to (1) the effects of urbanization in Denver and surrounding areas, and (2) the importation of water from the West Slope by transbasin diversions. Some of the changes in flow patterns can be seen in hydrographs spanning two separate periods from 1929-1957 and 2003-2015 (Figure 7). The record of discharge from 1929-1957 (Fig. 7a) shows a nearly natural hydrograph with prominent high flows during spring runoff, and extremely low flows during baseflow periods. The second hydrograph representing the period from 2003-2015 (Fig. 7b), shows that flows in this reach have been impacted by regional growth and water transfers. The most noticeable trend is in base flows, which are much higher now, even in times of regional drought (e.g. 2000-2006). The increase in baseflows can be attributed to return flows from irrigated areas and waste-water treatment plants, especially Denver metro. It can also be seen that the magnitude of peak flows in more recent years is slightly higher than those recorded half

a century earlier; whether this difference is large enough to have caused appreciable changes in channel morphology is difficult to determine without historical aerial photographs.

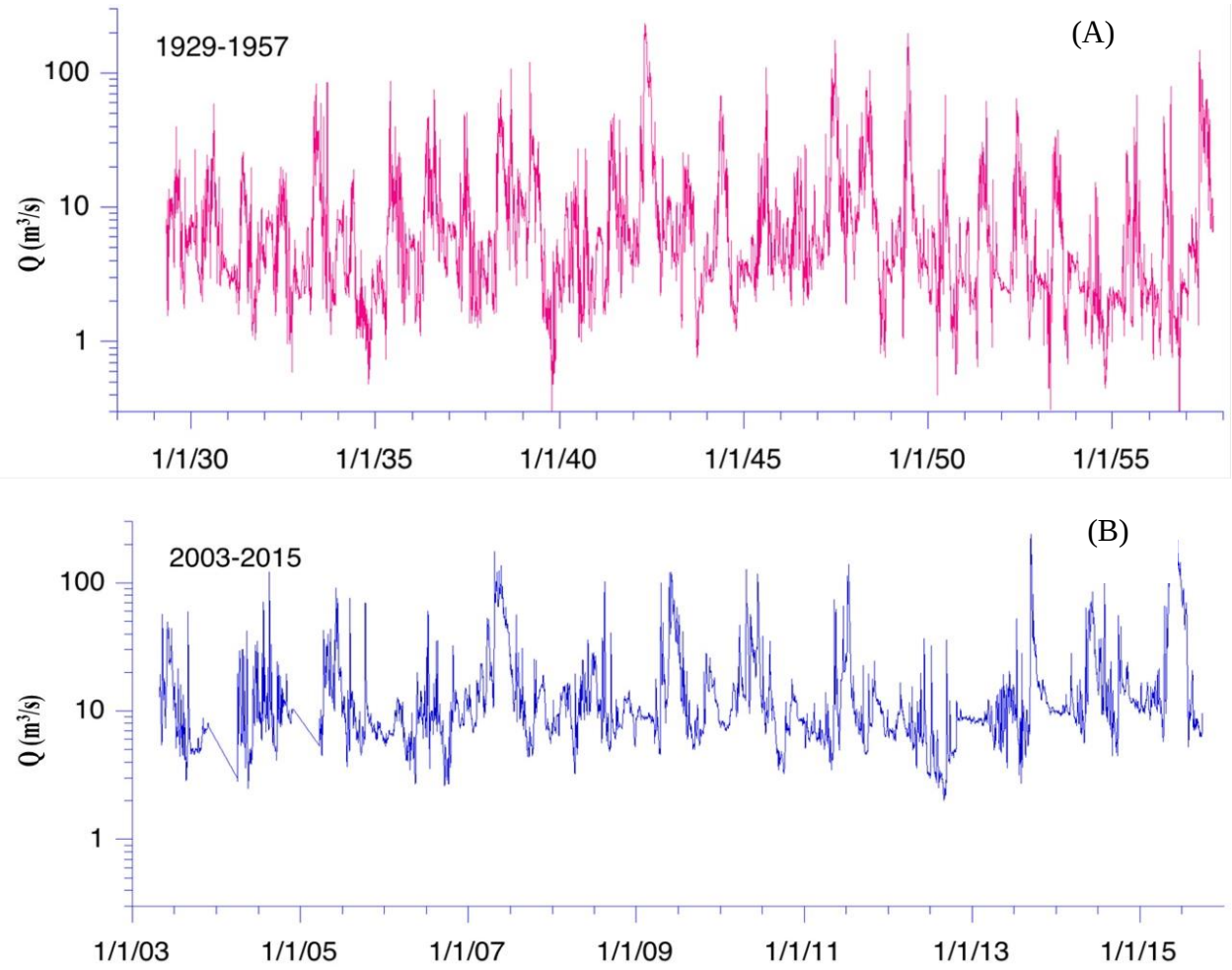


Figure 7. Hydrographs from USGS gauge station No. 06721000 just upstream (south) of the study area. The top hydrograph (a) shows discharge data between the years 1929-57 and represents a nearly natural channel while the bottom hydrograph (b) shows recorded data between

In many models of channel dynamics, a simulation is run using the bankfull flow, representing a peak discharge with a recurrence interval of 1-3 years. In early studies of bankfull flow frequency it was suggested that the bankfull discharge had a common recurrence interval of 1.5 years (Dury et al., 1963; Hickin, 1968; Leopold, 1994; Leopold et al., 1964), hence the two

flows have often been considered equivalent. However, results presented in subsequent work have shown that the recurrence interval for bankfull discharges could be much broader, with a range between 2-5 years (Castro and Jackson, 2001; Petit and Pauquet, 1997; Williams, 1978). For this study, a peak discharge with a 2-year return period was chosen as representative of bankfull flow conditions. Annual peak flow data for the Fort Lupton gauge were downloaded from the USGS web site, and used to plot the flood frequency curve shown in Figure 8. From this curve, the discharge corresponding to the 2-yr flood was estimated to be 113.2 $m^3/s$.

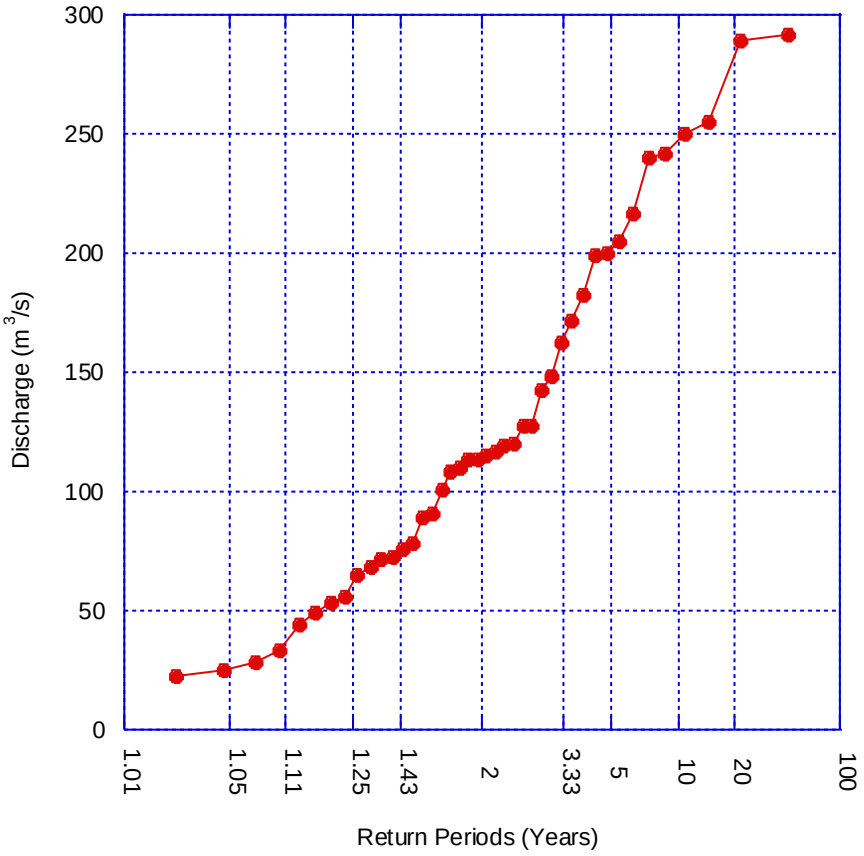


Figure 8. Flood frequency curve.

When considering the commonly used methods in the field of hydrology and geomorphology discussed in many of the papers mentioned in this section, a flow of 113.2 $m^3/s$

was chosen to represent the "bankfull" flow. Table 1 below summarizes the four flows chosen to model.

Table 1. Summary of discharges used to model, showing in-channel flow experienced at the study site (SS flow) after upstream diversions were subtracted from the gauge data.

| | Date | USGS ($ft^3/s$) | PVD ($ft^3/s$) | MID1 ($ft^3/s$) | SS Flow ($ft^3/s$) | SS Flow ($m^3/s$) |
|---|---|---|---|---|---|---|
| Low Flow | 10/17/2015 | 256.29 | 38.50 | 14.30 | 203.49 | 5.76 |
| Medium Flow | 8/17/2015 | 641.75 | 91.35 | 23.75 | 526.65 | 14.90 |
| High Flow | 7/14/2015 | 2415.00 | 84.30 | 23.80 | 2306.90 | 65.29 |
| Bankfull Flow | - | - | - | - | 4000 | 113.20 |

In the previous table, USGS represents gauging station 06721000, PVD represents the Platte Valley Diversion, MID1 represents Meadow Island Diversion No. 1, and SS Flow represents the flow experienced at the study site. All values represented in the table have been rounded to the nearest hundredth decimal point. From this point on, the four flow levels will be referred to as low flow, medium flow, high flow, and bankfull flow.

## 3.4 Flow Modeling

A key input into the FaSTMECH model is the downstream boundary stage. The model uses this value as an initial condition during the calculation procedure. Water Surface Elevations (WSE) were gathered during the low, medium, and high flow events at each of the XSs, from which a rating curve was made (Fig. 9). The fitted curve extends out to 10,300 cfs (291.49 cms) due to the fact that this is the highest recorded flow experienced at the study site.

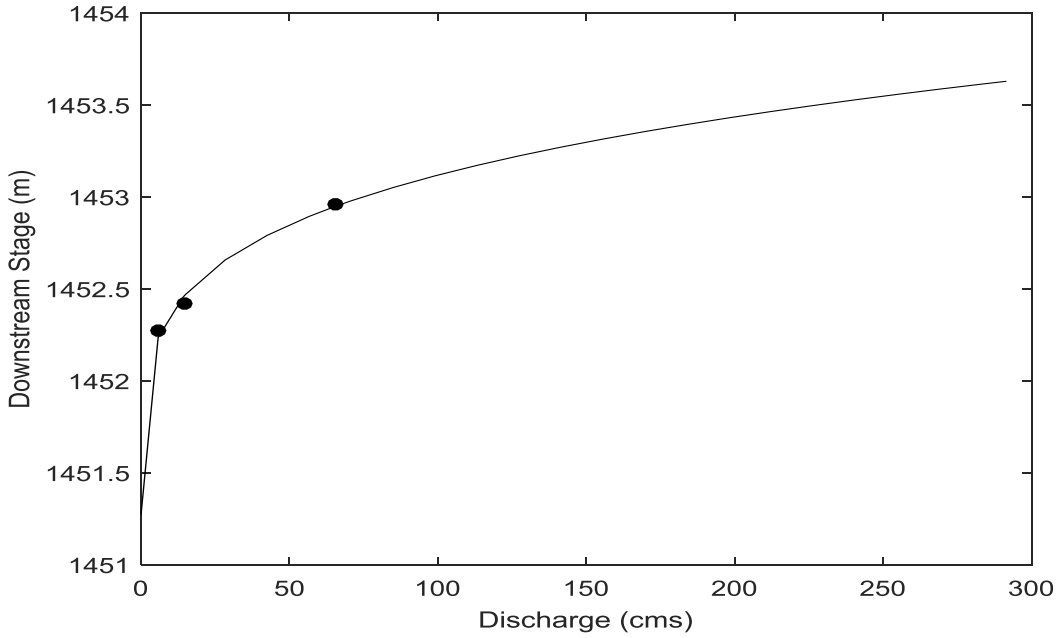


Figure 9. Rating curve for the downstream stage at the study area.

Equation 1 below shows the second order power function fit to the data points where downstream stage has units of meters and discharge has units of [$m^3/s$].

$$Downstream\ Stage = 0.647 * Q^{0.228} + 1451.27 \quad (1)$$

In order to acquire preliminary estimates of Manning's n values during the variable flow events, one dimensional HEC-RAS simulations were run. Channel geometry, river reach curvature, measured WSEs, and discharge data were all input into the program. The model was run by altering the Manning's n-value until model WSEs closely matched observed WSEs. The results of this process are presented in Appendix A.

## 3.5 2-D Modeling Software

The two-dimensional patterns of flow and sediment transport were simulated with the FaSTMECH (Flow and Sediment Transport with Morphologic Evolution of Channels) model, developed by the U.S. Geological Survey (USGS) (McDonald et al., 2006; Nelson et al., 2006, 2003). FaSTMECH uses a channel-centered orthogonal curvilinear grid to perform calculations (Nelson and Smith, 1989). The model computes both the down-stream and cross-stream components of water velocity (u and v, respectively) using a finite difference solution to depth-averaged and Reynolds-averaged momentum equations (Legleiter et al., 2011; Nelson et al., 2006). It assumes all flow to be both steady and hydrostatic while treating turbulence by relating the Reynolds stress to shear stresses via an eddy viscosity (Barton et al., 2005; Legleiter et al., 2011b; Logan et al., 2011). Additionally, the model uses both the two components of velocity (u and v) and an estimation of channel roughness (Cd) to calculate shear stresses (τ) in the down-stream (x) and cross-stream (y) directions (Nelson, 1999).

$$\tau_x = \rho C_d u \sqrt{(u^2 + v^2)} \tag{2a}$$

$$\tau_y = \rho C_d v \sqrt{(u^2 + v^2)} \tag{2b}$$

In these equations, ρ is the density of water, $C_d$ is a dimensionless drag coefficient, and u and v are the flow velocities in the down-stream and cross-stream directions, respectively.

FaSTMECH is a river flow / riverbed variation analysis solver which employs a curvilinear coordinate system for its lattice system. Due to the software's calculations under quasi-steady approximation, simulations with extremely long timeframes can be run. Additionally, FaSTMECH is unique in that it implements a Habitat Calculator, enabling it to evaluate river ecosystems by incorporating the calculated results of the obtained flow / riverbed variations. Primary inputs into the model include detailed topography, discharge, WSE at the

downstream end, and bed roughness, expressed as either a roughness length ($z_o$) or a drag coefficient ($C_d$) (Legleiter et al., 2011; Lisle et al., 2000; Segura and Pitlick, 2015). Bed stresses are calculated with the use of a drag coefficient closure (Nelson et al., 2003), which can be defined as constant or variable over time and space. For this study, the bed roughness was represented as a drag coefficient. Simulations were run with both uniform roughness (sandy bed forms) and variable roughness (representing varying density vegetation). Detailed field surveys provided the initial channel topography for the model (Figure 4). Aerial photography of the study area was then added to aid in the interpolation of elevation data. Interpolating points between measured topography helped to reduce the influence of irregularities in the topography that may form during the triangulation within FaSTMECH. A template mapping technique with user specified stream-wise and cross-stream distances was used to map elevation data to all points in between cross-sections.

### 3.5.1 Grid Creation

As previously mentioned, FaSTMECH uses a curvilinear grid system to perform calculations. The grid follows a user specified centerline, which for the purposes of this study, follows the center of the channel. The model domain extends the entire length of the study area (406 m) with a width of 150 m (Fig. 10). This width was chosen in order to incorporate both river banks, the entire large sand bar on the right (northern) bank, as well as a portion of floodplain on either side of the reach. The grid spacing was chosen to be approximately 1m x 1m, leading to a total of 57,246 nodes.

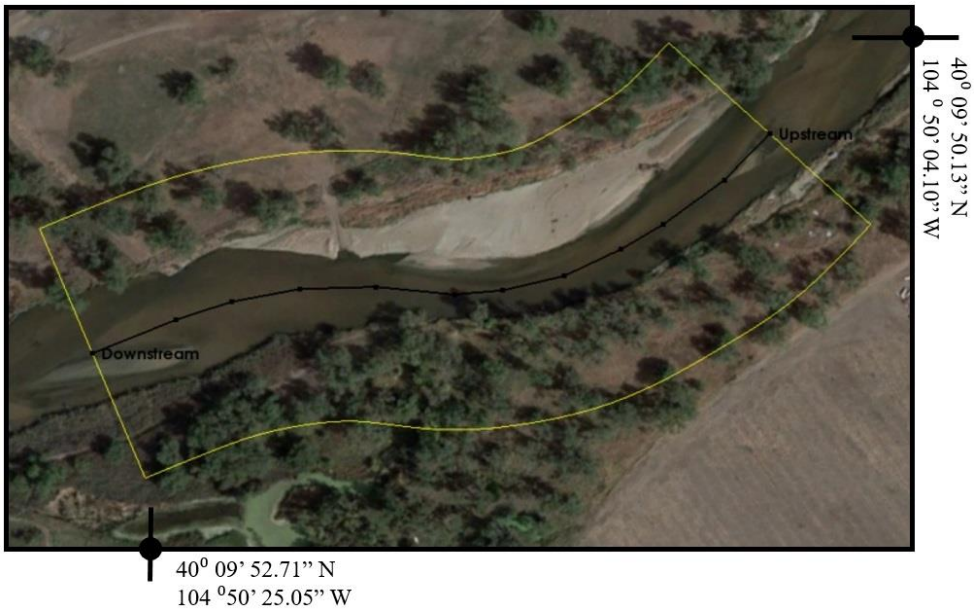


Figure 10. Grid boundary (yellow) with specified centerline following the middle of the channel.

### 3.5.2 Topographic Resolution

The mapped elevations generated from initial field surveys were supplemented with additional points to increase topographic resolution.

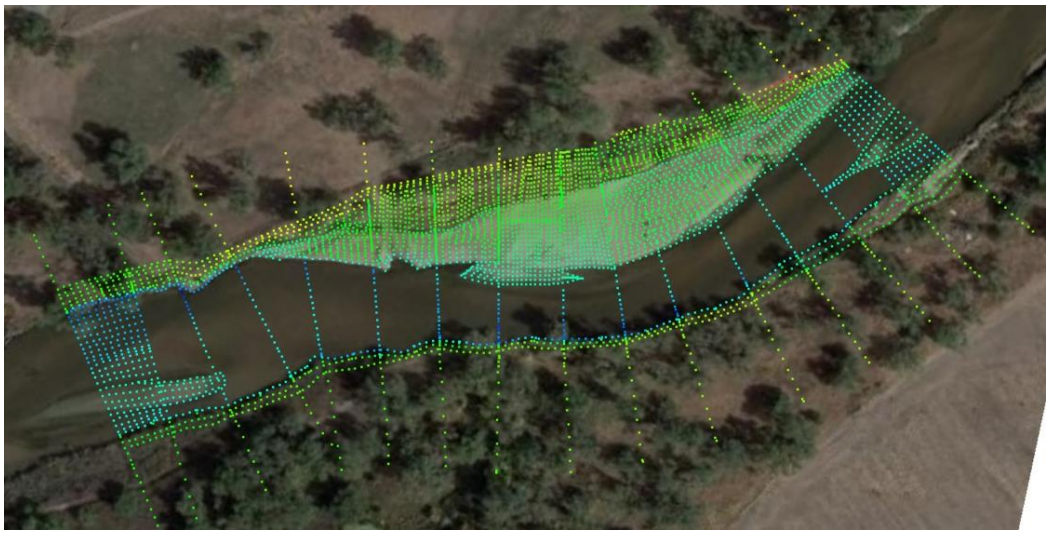

Figure 11. Locations of every elevation data point used. Additional points were added in between cross-sections, at very fine spacing on the large sand bar, and extending the cross-sections further onto the floodplain.

As shown in Figure 11, points were added surrounding the downstream and upstream boundaries and along the banks in order to provide better resolution and clarity for model simulations. The added points helped to ensure that the flow was both at the correct elevation and flowing in the proper direction. Increasing the resolution of the elevation data on the mid-channel bars was important for modelling differences in flow depth, particularly at low flows. Many data points were also interpolated on the surface of the large sand bar on the right bank as it is the main focus of this study. It is known that during higher discharges, the river flows over portions of this bar, affecting flow velocities, sediment transport rates, and shear stress distributions. In order to properly map the elevations of this bar, a centerline was drawn between the peak elevations of the bar at each cross-section it crossed. Elevations were then interpolated in the cross-stream direction starting from this centerline, leading to lower elevations near the edge of flow. Figure 12 below shows the final geographic data for the entire study area using the model's template mapping technique.

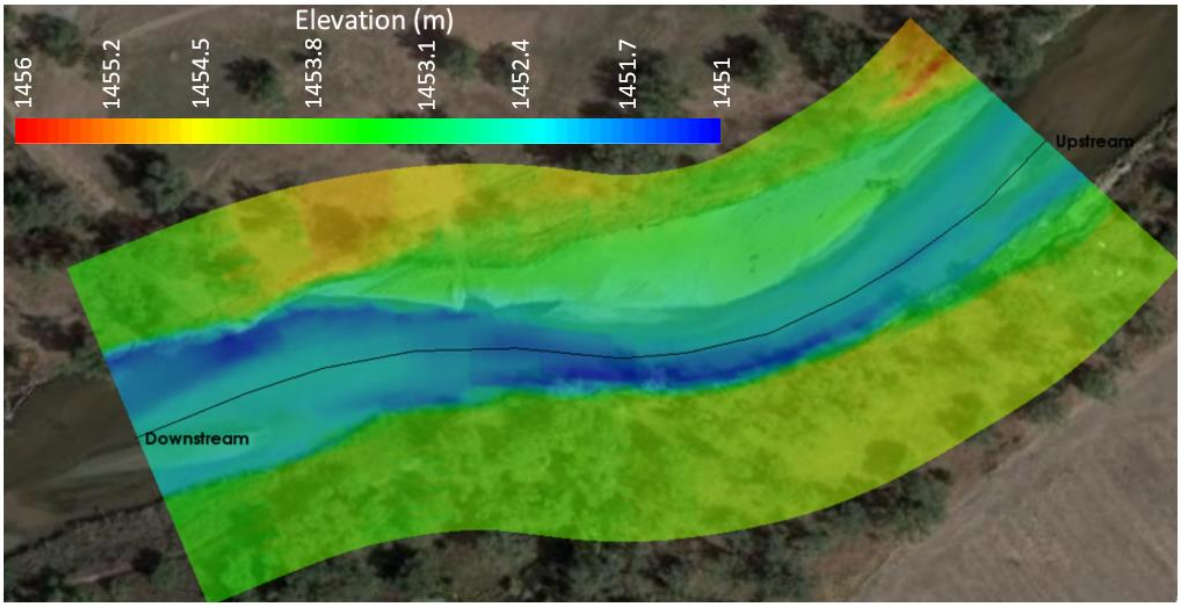


Figure 12. Model interpolated elevation data for the entire study area. All elevations are in meters above sea level.

### 3.5.3 Simulation Scenarios

In order to model the effects of vegetation on sediment transport rates and flow dynamics, four discharges ranging between 5-100% of bankfull flow ($Q_{bf}$) were chosen. Two different situations were modeled: a uniform roughness scenario, where the entire inundated area is assumed to have equal roughness, and a variable roughness scenario, where the study area is partitioned into two separate parts, a bed roughness and a vegetation roughness. Based on observations in the field, the low and medium discharges (5.76 and 14.9 $m^3/s$, respectively) never over-topped the large sand bar on the northern bank or the vegetated floodplain areas. Due to this fact, only the two highest flows (65.29 and 113.2 $m^3/s$) were modeled in the variable roughness simulations. A more detailed analysis for setting up the variable roughness simulations is discussed in section 3.5.5.

### 3.5.4 Model Calibration – Uniform Roughness

In order to quantify the results of variable roughness simulations (representing the implementation of riparian vegetation), four different flow simulations with uniform roughness were run for comparison purposes. These simulations represent an idealized situation where the bed roughness throughout wetted portions of the channel are uniform. The model was calibrated by adjusting two tunable parameters, the dimensionless drag coefficient ($C_d$) and the lateral eddy viscosity (LEV). The dimensionless drag coefficient is calculated as:

$$C_d = \frac{n^2 g}{\bar{h}^{1/3}} \quad , \tag{3}$$

where n is the Manning's n value, g is the gravitational constant, and $\bar{h}$ is the mean flow depth. The drag coefficient can be either constant in space or spatially variable. For these simulations, the bed material is assumed to be uniform and thus the drag coefficient is assumed to also be uniform in space.

The second parameter, LEV, is a measure of lateral momentum exchange. It is a correction to the eddy viscosity used in the vertically averaged equations to treat lateral separation eddies. The LEV can be estimated as follows:

$$LEV = (0.01 - 0.001)\bar{h}\bar{u} \quad , \tag{4}$$

where $\bar{u}$ represents the mean flow velocity.

Calibration then consisted of adjusting the values of these two parameters to match the calculated WSE and the observed WSE. This iterative process was repeated until the lowest RMSE was achieved. Values for $C_d$ ranged from 0.004-0.006, which is equivalent to Manning's n values ranging between 0.0179-0.028 for typical depth scales of the reach. These values correlate closely with the initial estimates for Manning's roughness coefficient (n) obtained in preliminary 1-D model runs with a one-dimensional flow (HEC-RAS) model. It was found that the FaSTMECH model results were not very sensitive to LEV values, which ranged from 0.015-0.05. A previous study reported a 2-fold range in LEV values used without altering the model predictions (Legleiter et al., 2011b). Both of these calibrated values ($C_d$ and LEV) align closely with those reported in other studies (Barton et al., 2005; Legleiter et al., 2011b; Logan et al., 2011; Mueller, 2012; Rossi, 2014; Segura and Pitlick, 2015).

FaSTMECH also incorporates the use of three relaxation coefficients. For this study, both the relaxation coefficient for velocity (URelax) and the adjustment for the global slope of the

WSE at each iteration (ARelax) were kept as the default values. However, when necessary, slight adjustments were made to the relaxation coefficient for WSE (ERelax) in order to help match WSE values.

Calibration was conducted until the lowest Root Mean Squared Error (RMSE) value between measured and modeled WSE was reached. The RMSE is calculated according to the equation below.

$$RMSE = \sqrt{\frac{1}{n}\sum_{i=1}^{n}(\hat{y}_i - y_i)^2} \quad (5)$$

In this equation, $\hat{y}_i$ denotes the predicted value for the ith observation and $y_i$ denotes the observed value for the ith observation. In this scenario, if the model perfectly predicted the measured WSEs, the RMSE would be zero. Table 2 shows the final values of all important model parameters and the RMSE of each uniform roughness simulation.

Table 2. Model results for uniform roughness simulations. Downstream stage represents the WSE elevation at the downstream boundary input as an initial condition. $Q_i/Q_{bf}$ represents the fraction of bankfull flow experienced at a particular flow level.

| Uniform Roughness / Flow Level | Q ($m^3/s$) | Downstream Stage (I.C.) (m) | $C_d$ (-) | LEV ($m^2/s$) | $U_{relax}$ | $A_{relax}$ | $E_{relax}$ | RMSE | $Q_i/Q_{bf}$ |
|---|---|---|---|---|---|---|---|---|---|
| Low Flow | 5.76 | 1452.27 | 0.006 | 0.05 | 0.2 | 0.2 | 0.4 | 0.028 | 0.05 |
| Medium Flow | 14.9 | 1452.42 | 0.004 | 0.015 | 0.2 | 0.2 | 0.3 | 0.054 | 0.13 |
| High Flow | 65.29 | 1452.96 | 0.005 | 0.045 | 0.2 | 0.2 | 0.4 | 0.022 | 0.58 |
| Bankfull Flow | 113.2 | 1453.17 | 0.005 | 0.045 | 0.2 | 0.2 | 0.2 | - | 1.00 |

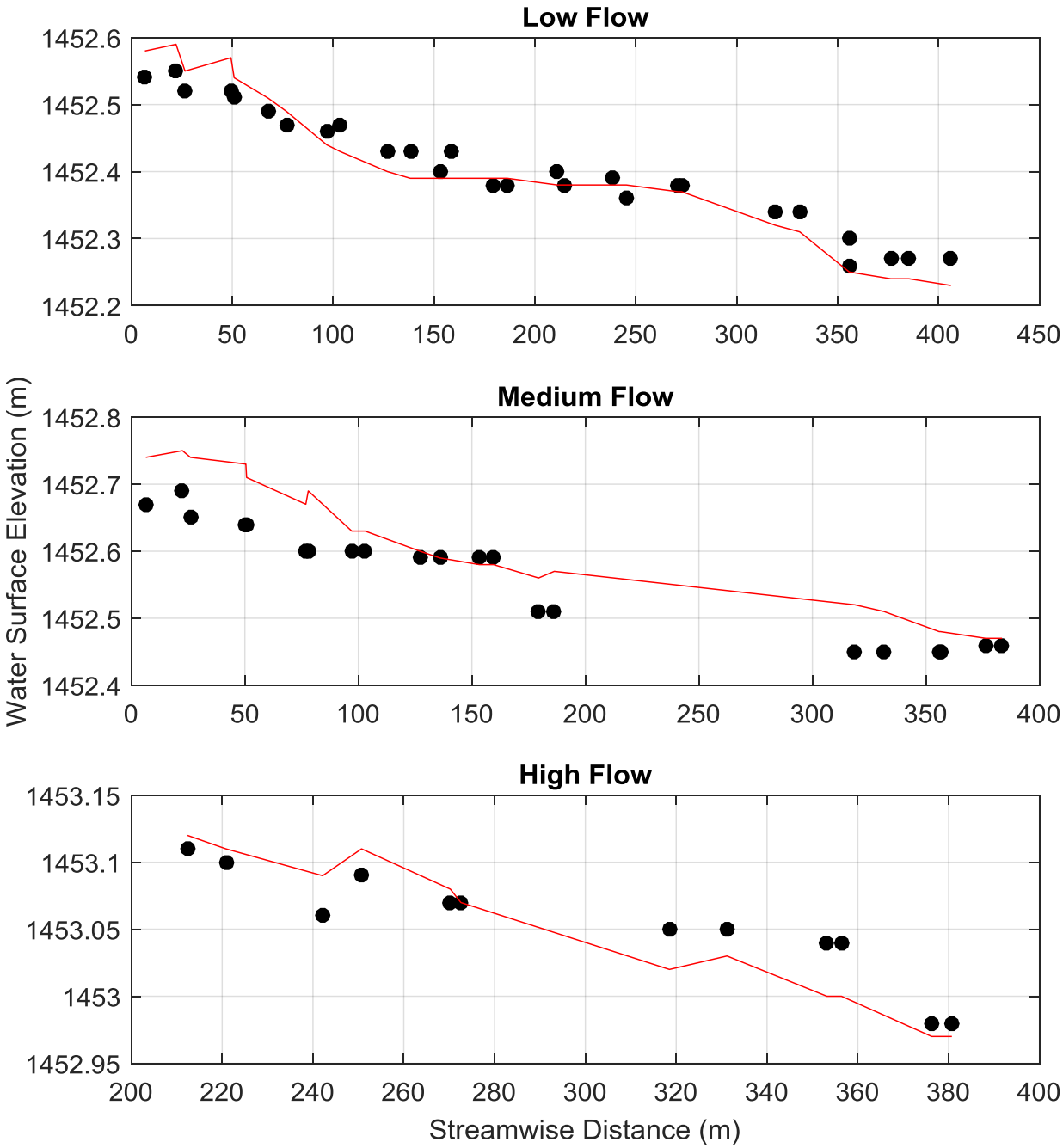


Figure 13. Comparison of observed (black dots) and calculated (red lines) water surface elevations for uniform roughness simulations. Notice both the x and y scales are different in order to better show the data. Due to dense vegetation, measurements of WSE during the high flow scenario were only able to be taken for half the reach.

Figure 13 shows a comparison of observed and calculated water surface elevations. Additionally, the RMSE values associated with each simulation can be found in Table 2. Being that there were no field measurements taken for the bankfull flow because the associated flow level was never experienced during the duration of this study, there were no observed WSE data to compare with simulated WSE. Furthermore, the values for roughness coefficient and lateral eddy viscosity for the bankfull flow simulation were set equal to the values found during the high flow calibration. It can also be seen that the range of values for streamwise distance vary with each situation. This is due to a lack of gathered WSE data at certain cross-sections of the reach due to very thick and dense vegetation during the time of field surveying. However, there still remains sufficient enough data to properly calibrate the FaSTMECH model.

### 3.5.5 Vegetation Roughness Characteristics

Although there currently does not exist any vegetation on the large sand bar on the north bank of the study site, it is reasonable to assume that willow may spread from the river banks onto the large sand bar during extended periods of low flow (drought). Estimates of roughness representing the presence of vegetation were made on the basis of results from previous studies. As previously mentioned, FaSTMECH represents roughness as a dimensionless drag coefficient, and the model has the capability to separate bed roughness from vegetation roughness. Both terms are dependent on the mean flow depth ($\bar{h}$) and Manning's n. With data gathered from field surveys, the mean flow depth at three different discharges was known. However, with the use of a 1-D HEC-RAS model, only estimates for Manning's roughness coefficient associated with bed material (ranging between 0.0185-0.034) had been attained. To acquire estimates for riparian

vegetation, a USGS guide for selecting Manning's roughness coefficients was used (Arcement and Schneider, 1989). These authors present a method for determining n-values for densely vegetated floodplains by choosing roughness values for multiple criteria describing the floodplain and adding these values to a base roughness representative of bed material. The final value for the composite roughness of vegetated areas is:

$$n_{floodplain} = n_b + n_1 + n_2 + n_3 \quad (6)$$

In this equation, $n_{floodplain}$ represents the final adjusted Manning's roughness coefficient representing the vegetated surface, $n_b$ represents the Manning's n associated with the bed material of the reach and found during calibration of the uniform roughness scenario, $n_1$ represents the adjustment value for irregularities in the shape of the surface (in regards to rises, dips, sloughs, etc.), $n_2$ represents the variation of the cross section (set equal to zero for most cases), and $n_3$ represents the adjustment value for effects of obstructions (in the form of debris, deposits, stumps, logs, exposed roots, or isolated boulders) on the surface of the floodplain. Based on information presented in Arcement and Schneider, (1989), values of $n_1$, $n_2$, and $n_3$ were set to 0.008, 0, and 0.012, respectively. Therefore, the final estimated Manning's roughness coefficient representing the vegetated areas was estimated to be 0.042. For the bankfull flow scenario (133.20 $m^3/s$) where the average depth over the sand bar of interest on the northern bank was 0.40 meters, $C_d$ was calculated to be 0.0235.

Finally, a value for Manning's roughness coefficient representative of the willow vegetation on the river banks was estimated to be 0.10. The description for this value states, "…the average depth of flow is below branches or… moderate to dense bushy willow" (Arcement and Schneider, 1989). Both of these statements hold true for the study site. For the accompanying flow depth during the high flow discharge, a $C_d$ value of 0.133 was calculated.

The large sand bar on the north side of the channel was not over-topped during the low flow (5.76 $m^3/s$) or medium flow (14.90 $m^3/s$) levels, therefore, only the two higher flow levels were modeled for the variable roughness scenario.

Table 3. Summary of Cd values used in every simulation, both uniform and variable roughness scenarios. Notice that the vegetation roughness over the floodplain was set equal to zero for the uniform roughness scenarios. It was also assumed that there was no in-channel vegetation.

| Flow Level | Q ($m^3/s$) | $C_d$ (channel) | $C_d$ (floodplain) | $C_{d,veg}$ (channel) | $C_{d,veg}$ (floodplain) |
|---|---|---|---|---|---|
| *Uniform Roughness* | | | | | |
| Low Flow | 5.76 | 0.006 | 0.006 | - | - |
| Medium Flow | 14.90 | 0.004 | 0.004 | - | - |
| High Flow | 65.29 | 0.005 | 0.005 | - | - |
| Bankfull Flow | 113.20 | 0.005 | 0.005 | - | - |
| *Variable Roughness* | | | | | |
| High Flow | 65.29 | 0.005 | 0.0235 | - | 0.133 |
| Bankfull Flow | 113.20 | 0.005 | 0.0235 | - | 0.133 |

Figure 14. Highlighted regions of variable roughness caused by vegetation within the study area.

In Figure 14, the red regions represent the variable roughness zones. Within these regions, both the vegetation roughness and the base roughness differ from that of the main channel. The extent of these differences can be seen in Table 3. The variable roughness regions extend past the model grid boundaries only to ensure that all the edges of the grid have been accounted for. Furthermore, at the upstream boundary, the variable roughness zones were chosen to point outwards towards the floodplain. This adjustment allows the model a period to first equilibrate to the flow before it is affected by variations in roughness.

Because there was no vegetation growth on the sand bars when the field surveys were conducted, there is no physical data representative of the model scenario that calculated results could be compared to. Therefore, the estimates of Manning's roughness coefficients, which were converted into a dimensionless drag coefficient, were assumed to be representative of the physical environment.

# 4 RESULTS

## 4.1 Model Outputs

For the main part of this study, 6 simulations were run; 4 different discharge levels for an ideal uniform roughness scenario and 2 higher flows for a variable roughness situation, representing the implementation of riparian vegetation. For modeling purposes, it was assumed that the discharge during each simulation was uniform in space and steady in time, and that the grain size distribution was the same everywhere across the channel bed. The model results discussed in the subsequent pages represent a single instance in time given the initial conditions, boundary conditions, and input model parameter values.

Maps showing simulated patterns of depth, velocity and shear stress are presented in Figures 15-17. These simulations were run for four discharge levels assuming no vegetation was present within the channel. The maps of depth (Figure 15) show that, at low discharges, the flow is split around two small bars located at the upstream and downstream ends of the study reach. These bars are completely inundated at higher flows. Water begins flowing over the large bar on the north side of the channel at a discharge of 65.29 $m^3/s$, and the bar is nearly completely inundated at a discharge of 113.2 $m^3/s$. At all discharges, flow is deepest in the area across from the large bar, where a prominent pool has formed along the south bank; depths are also high in the area along the north bank across from the smaller bar in the downstream end of the reach. The maps of velocity (Figure 16) generally follow the maps of depth, however, the highest velocities are not always associated with the deepest flows. At low discharges, velocities are highest in the areas upstream of the pools, whereas at high discharges the pattern shifts such that velocities are highest in the areas downstream of the pools. The maps of shear stress (Figure 17)

follow the maps of velocity relatively closely, although this is somewhat difficult to see given the difference in scales. The two variables are, however, closely related (see eqns. 2a, 2b), thus the zones of high and low shear stress generally correspond to zones of high and low velocity.

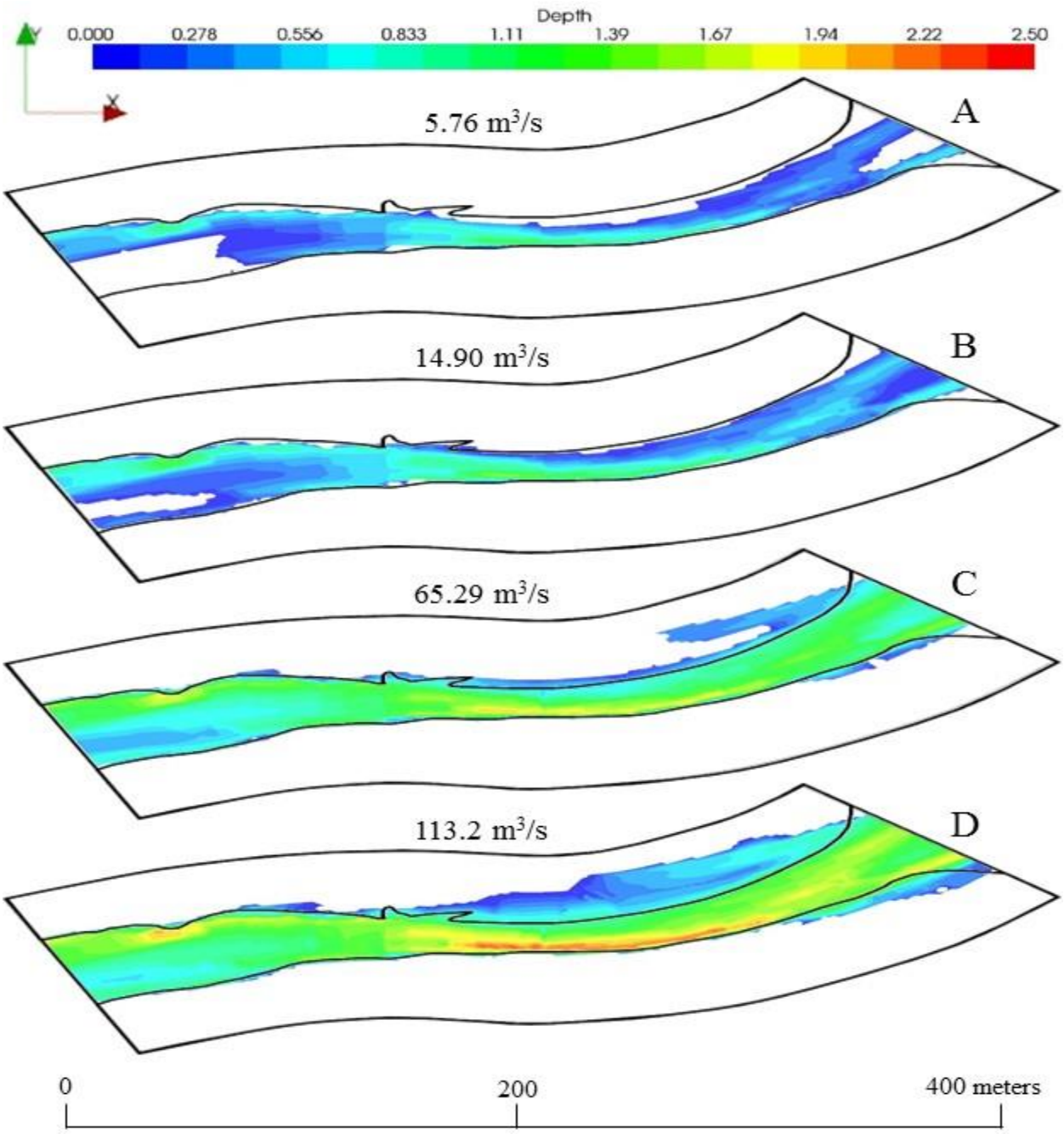


Figure 15. Maps of modeled depth [m] for the four uniform roughness scenarios. Notice the small side channel on the northern bank that begins flowing at Q=65.29 $m^3/s$ (C) and notice how the majority of the large sand bar is covered by the large flows in map D.

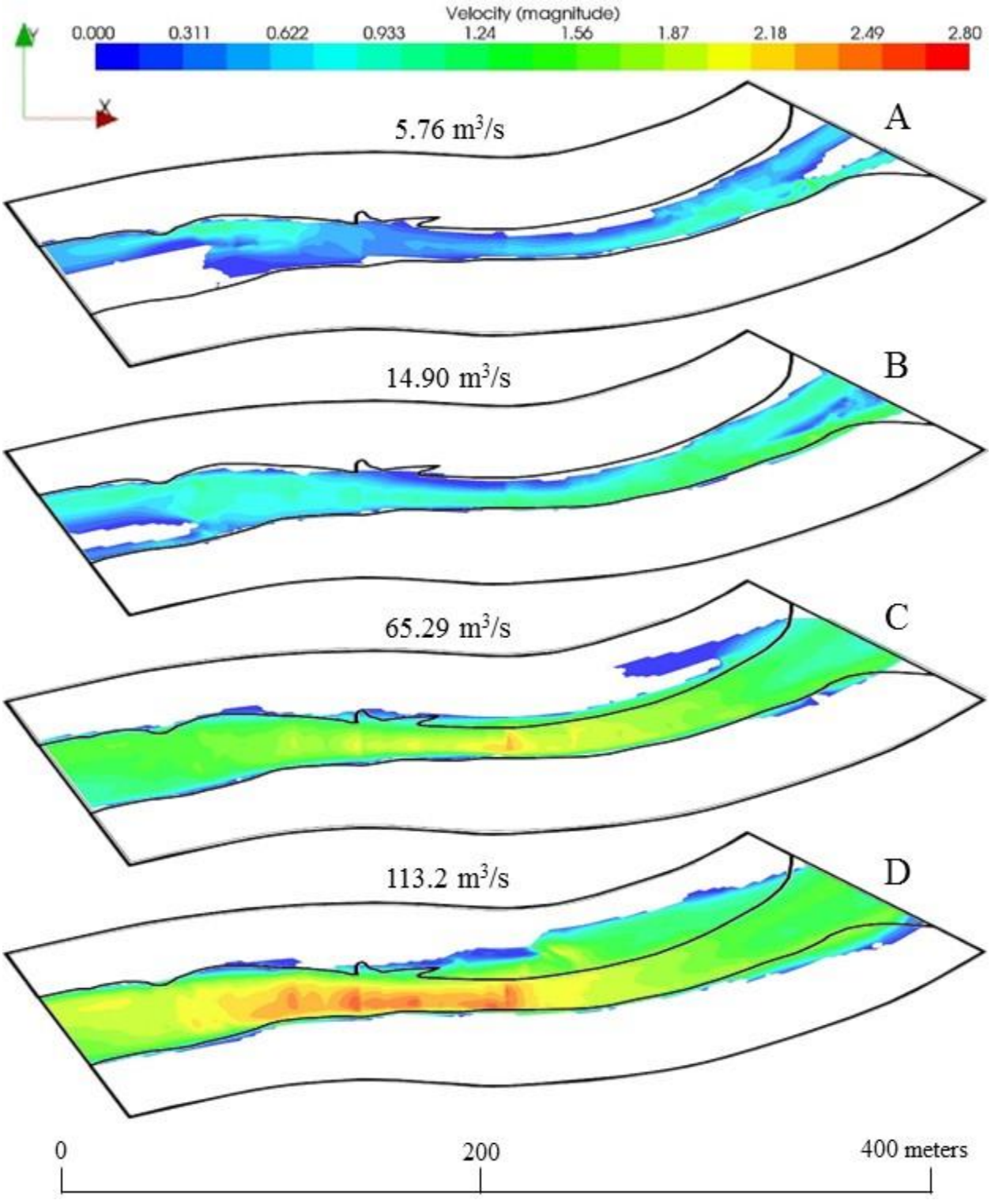


Figure 16. Model maps of flow velocity [m/s] for all the uniform roughness scenarios. It is clear to see that as discharge levels rise, the flow velocity within the main channel grows faster and faster. Additionally, the flow velocities over the large sand bar a

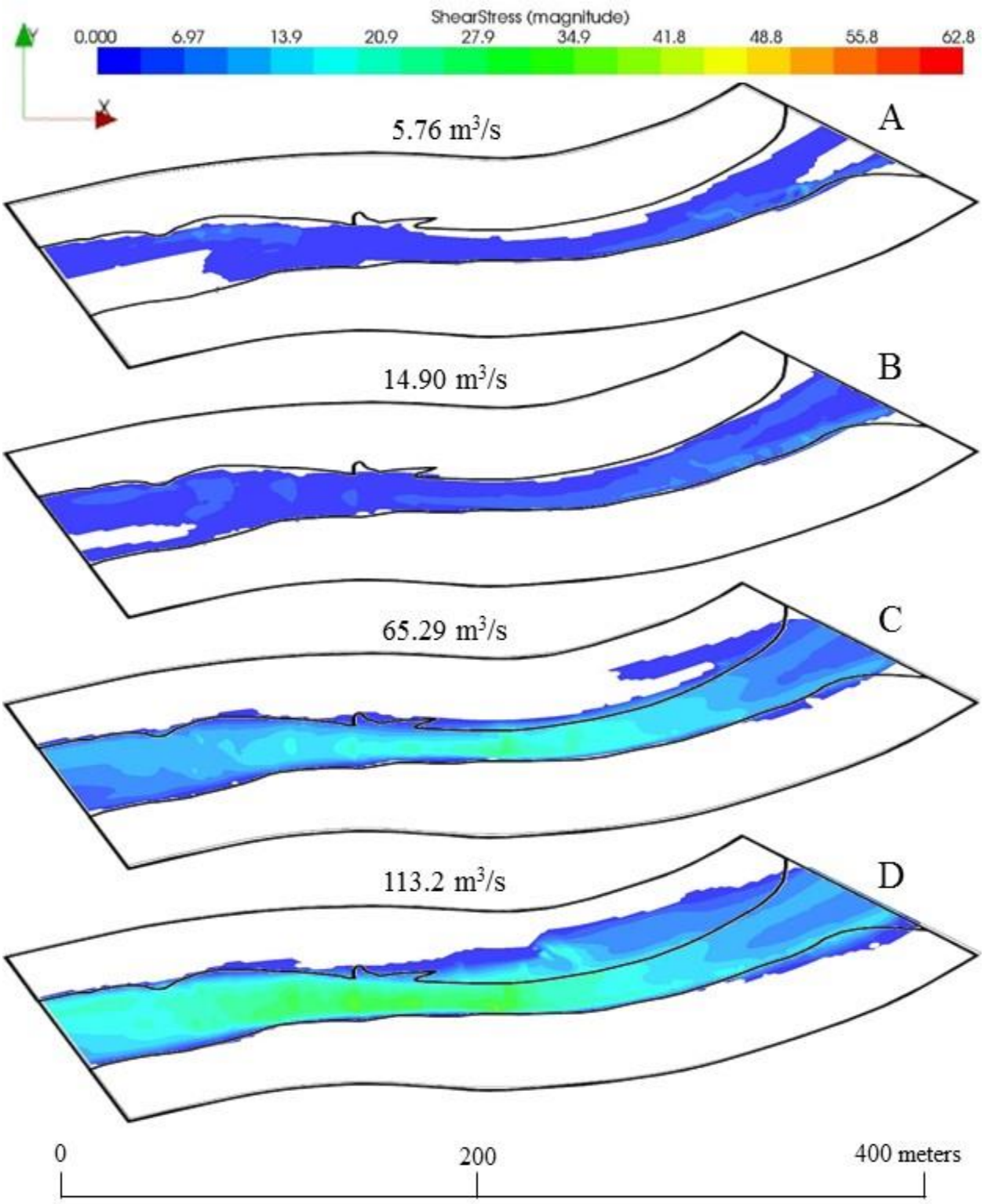


Figure 17. Model output maps of shear stress [$N/m^2$] for all the uniform roughness scenarios. Areas of larger shear stresses within the main channel closely correlate to areas with higher flow velocities.

Maps illustrating the effects of vegetation cover are presented in Figures 18-20 for the two discharges that over-topped the bar along the north side of the channel. In each of these figures, the top two panels, (A) and (B), compare uniform and variable roughness scenarios for a discharge of 65.29 $m^3/s$, while the bottom two panels, (C) and (D), compare uniform and variable roughness scenarios for a discharge of 113.2 $m^3/s$. The maps of depth (Figure 18) show that the largest increases in depth caused by vegetation occur around the in-channel bars located near the upstream and downstream boundaries, as well as the deepest areas of the channel across from the large sand bar and along the northern bank at the downstream side. The average flow depth throughout the reach, including the flow over the inundated sand bars, increases by as much as 10 cm when vegetation is present. The maps of velocity (Figure 19) show a very different pattern than the maps of depth with significant increases in flow velocities in the main channel, specifically occurring downstream of the deep pools. It can be seen that when vegetation is present on the large bar, the velocity on the bar decreases by more than 1 m/s. The increased drag, or resistance to flow, experienced on the bar diverts flow toward the main channel, increasing the velocity there. In contrast, the flow velocity near the banks of the main channel decreases slightly with increased vegetation, perhaps due to the roughness of the banks causing increased drag forces. The maps of shear stress (Figure 20) again follow the maps of velocity relatively closely, with the highest magnitude shear stresses occurring in regions with higher velocities. Shear stresses along the banks are relatively small compared to those in the middle of the channel, again likely due to larger drag forces caused by the roughness of the banks. Shear stresses across the large sand bar drastically decrease, leading to the conclusion that the majority of the sediment transport will occur in the main channel.

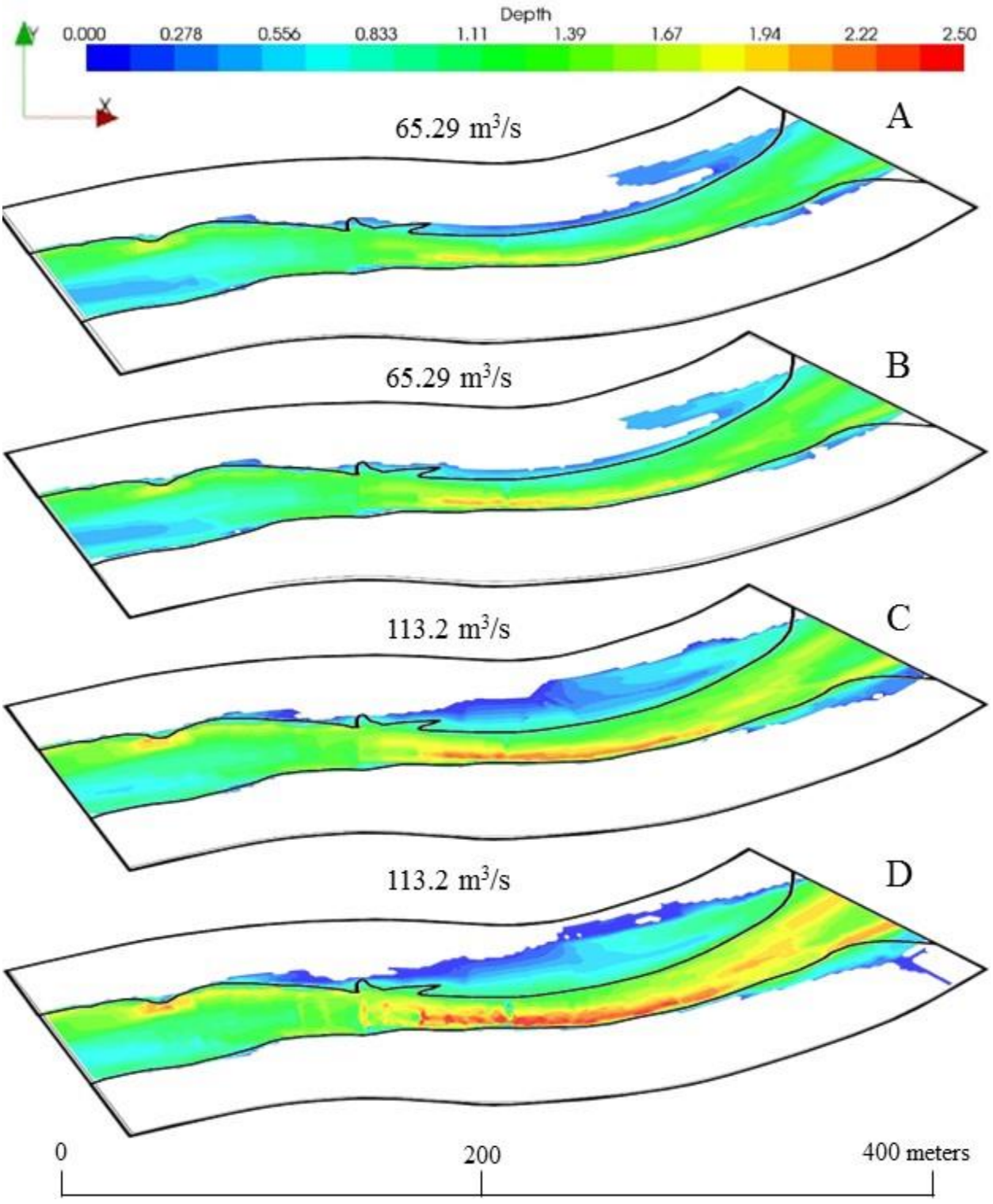


Figure 18. Modeled maps of depth [m] for the two discharges that over-top the northern bar, with their comparative uniform roughness maps. Maps A & C represent uniform roughness, while maps B & D represent variable roughness.

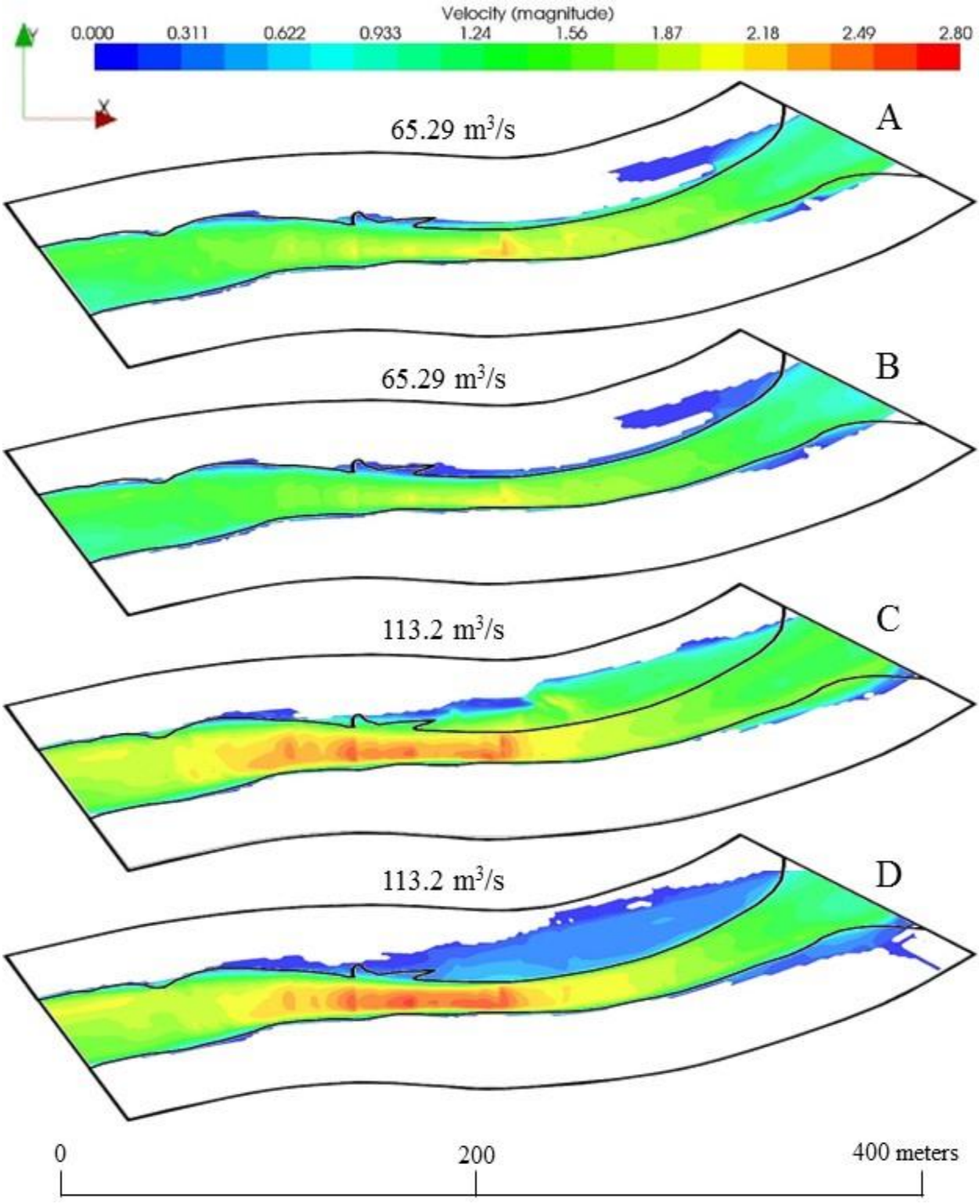


Figure 19. Modeled maps of flow velocity [m/s], comparing the uniform and variable roughness scenarios. Maps A & C represent uniform roughness, while maps B & D represent variable roughness.

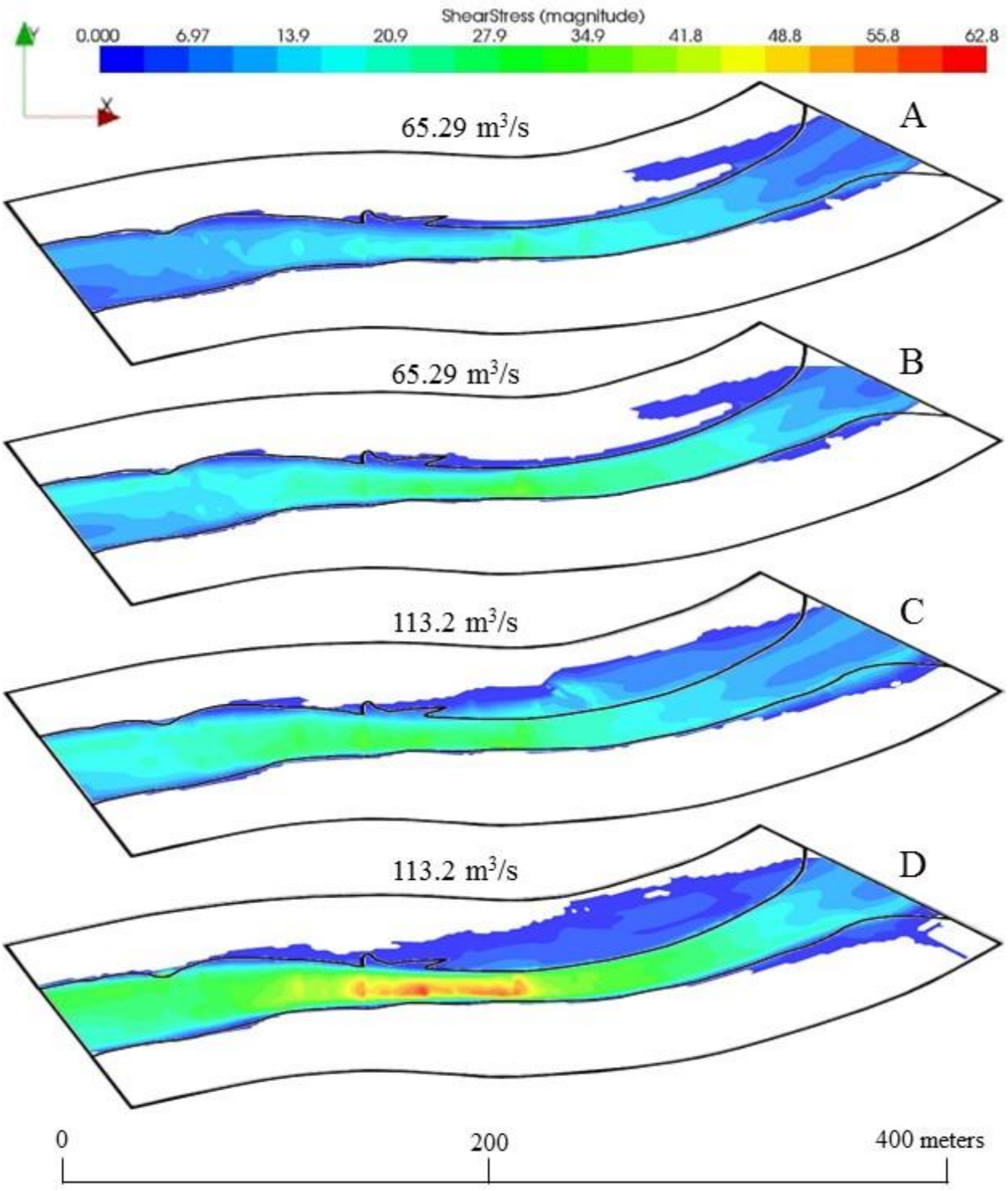


Figure 20. Modeled maps of shear stress [N/m$^2$], comparing the uniform and variable roughness scenarios. Maps A & C represent uniform roughness, while maps B & D represent variable roughness.

Table 4 below summarizes some of the values associated with the model outputs. As was previously discussed, the average depth throughout the reach increases by as much as 10 cm when vegetation is present. However, the mean flow velocity throughout the reach decreases with vegetation present. This is due to a drastic decrease in velocities over the large sand bar caused by increases in flow resistance. Distributions of shear stresses throughout the reach during different simulations will be discussed in the subsequent section.

Table 4. Depth and velocity model outputs for each simulation, broken down by discharge, fraction of bankfull flow, and roughness type.

| Roughness / Flow Level | Qi ($m^3/s$) | $Q_i / Q_{bf}$ | $H_{mean}$ (m) | $U_{mean}$ (m/s) | $U_{max}$ (m/s) | $RMSE_{WSE}$ (m) |
|---|---|---|---|---|---|---|
| Uniform Roughness | | | | | | |
| Low Flow | 5.76 | 0.05 | 0.39 | 0.51 | 1.55 | 0.028 |
| Medium Flow | 14.9 | 0.13 | 0.48 | 0.76 | 1.77 | 0.054 |
| High Flow | 65.29 | 0.58 | 0.93 | 1.30 | 2.33 | 0.022 |
| Bankfull Flow | 113.2 | 1.00 | 1.05 | 1.51 | 2.65 | - |
| Variable Roughness | | | | | | |
| High Flow | 65.29 | 0.58 | 1.02 | 1.13 | 2.16 | - |
| Bankfull Flow | 113.2 | 1.00 | 1.15 | 1.16 | 2.80 | - |

## 4.2 Shear Stress Distributions

In this section, a more detailed analysis of the patterns of shear stress extracted from model simulations is presented. It is evident from the results presented in the previous section that as the discharge through the study reach increases, the range in shear stresses experienced increases, as do the mean and median values (Table 5).

Table 5. Statistics of model output shear stress distributions for varying flow levels.

| Roughness / Flow Level | Q ($m^3/s$) | $\tau_{mean}$ ($N/m^2$) | $\tau_{median}$ ($N/m^2$) | $\tau_{sd}$ ($N/m^2$) | $\tau_{max}$ ($N/m^2$) | No. of Wet Nodes |
|---|---|---|---|---|---|---|
| Uniform Roughness | | | | | | |
| Low Flow | 5.76 | 1.94 | 1.42 | 1.74 | 16.68 | 10660 |
| Medium Flow | 14.9 | 2.71 | 2.57 | 1.89 | 12.02 | 14253 |
| High Flow | 65.29 | 9.47 | 9.59 | 5.24 | 27.48 | 19122 |
| Bankfull Flow | 113.2 | 13.09 | 12.55 | 7.69 | 37.82 | 24455 |
| Variable Roughness | | | | | | |
| High Flow | 65.29 | 12.56 | 12.92 | 7.80 | 38.02 | 19451 |
| Bankfull Flow | 113.2 | 16.23 | 12.68 | 14.14 | 62.77 | 26292 |

Additionally, as the discharge increases, a larger portion of the study area is represented by "wet" grid cells, leading to a much larger number of shear stress values when compared to low flows. These differences are illustrated in Figure 21 by a series of box plots showing the distribution of shear stress for each of the simulated flow scenarios.

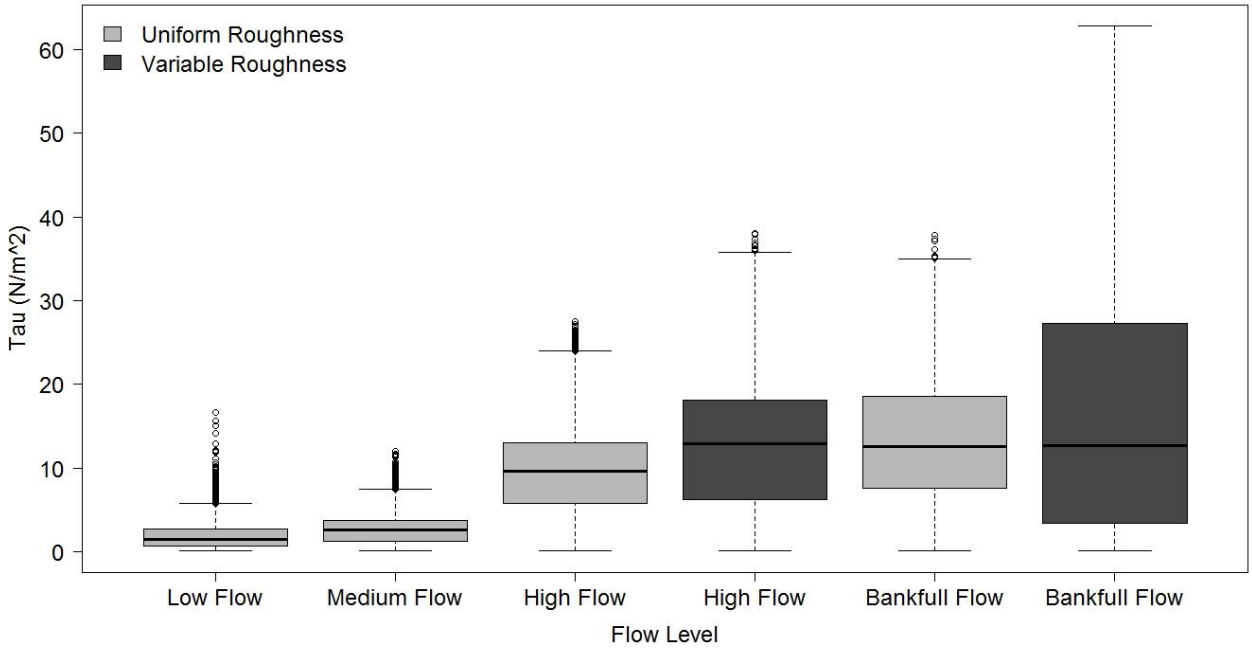


Figure 21. Boxplots of model output shear stress values for each simulation. The discharges represented are characteristic of low (5.76 $m^3/s$), medium (14.90 $m^3/s$), high (65.29 $m^3/s$), and bankfull (113.20 $m^3/s$) flow levels.

For the uniform roughness scenarios, the changes in flow level result in a gradual transition in the median and interquartile range of shear stress, with most of this transition related to changes in velocity in the main channel, rather than over the large sand bar. It can be seen that the variable roughness scenarios are characterized by larger magnitude shear stresses when comparing the distributions of shear stress for the same discharges but different roughness scenarios. Although the median values are similar, there exists a much larger proportion of shear stresses with higher magnitudes for the variable roughness simulations. These differences show that the growth of riparian vegetation has large effects on the flow over the large sand bar as well as the main channel. Figures 19 and 20 show that once vegetation is introduced into the model, the velocities and shear stresses over the large sand bar decrease drastically, while the velocities and shear stresses in the main channel increase drastically. This has important implications for sediment transport because transport is a nonlinear function of shear stress, therefore, a distribution with a higher proportion of large shear stresses will lead to much larger sediment transport rates than a distribution with a narrow range of stresses.

In order to best compare the distributions of shear stresses knowing that the statistics of the data at different flow levels vary, each distribution was normalized by dividing by its mean value, $< \tau >$. If a distribution is characteristic of a higher percentage of large shear stresses, it is likely that there will be more sediment transport. Histograms of the mean-normalized shear stresses representing the uniform roughness scenario are presented in Figure 22.

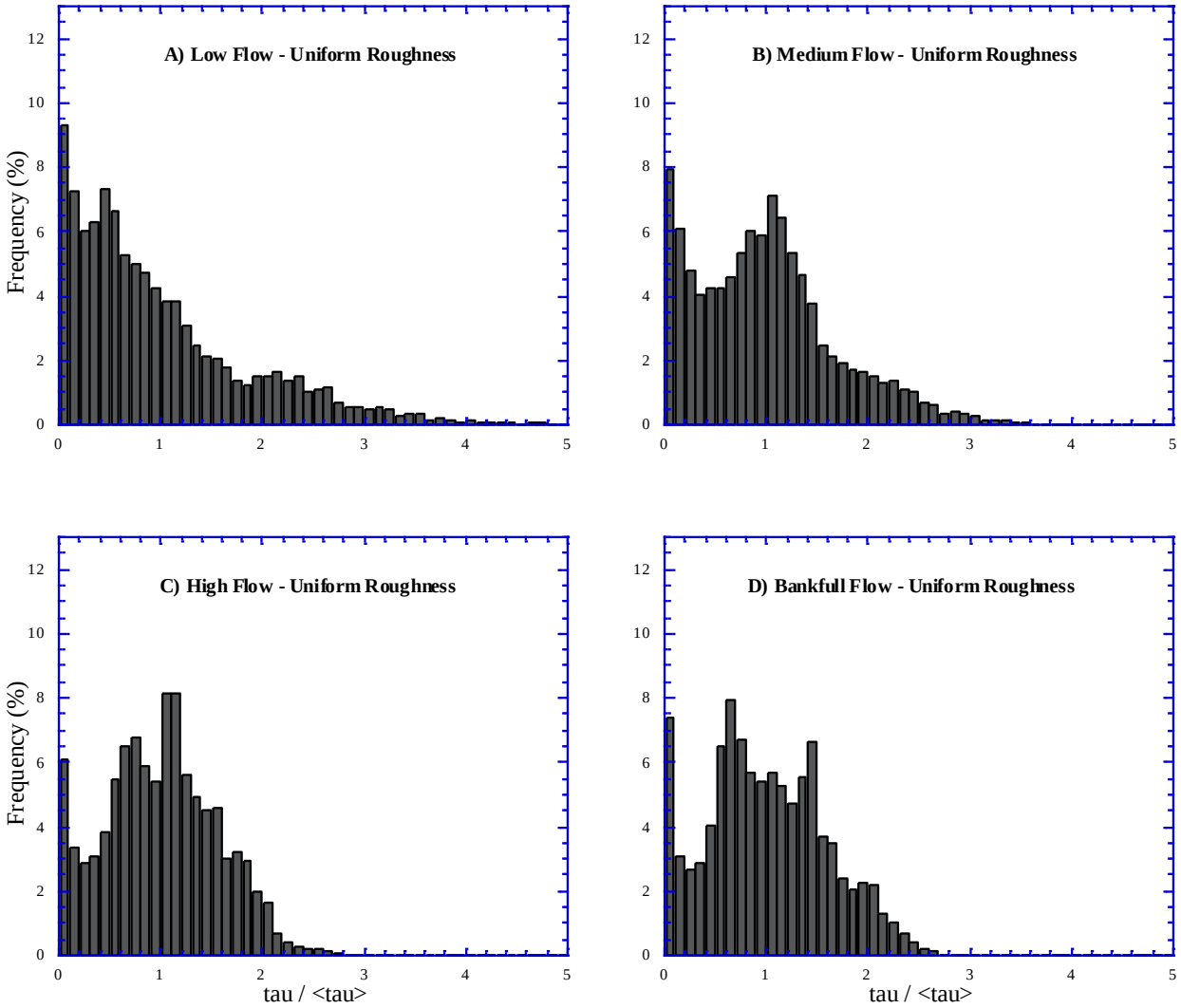


Figure 22. Histograms of mean-normalized shear stress distributions for the four uniform roughness scenarios.

We see from the histograms of uniform roughness that with increased flow levels, the distribution of shear stresses becomes more symmetric. At low discharges, the shear stress distribution is right skewed, characteristic of a large frequency of low shear stresses. However, the mean shear stress is substantially smaller for the lower flows than the large flow events. The range of the normalized shear stress distributions also changes with the discharge, becoming narrower as flow increases. For the lowest flow level (.05 $Q_{bf}$), the range in $\tau$ is up to 5 times $< \tau >$, whereas the highest modeled flow, bankfull flow ($Q_{bf}$), shows a range in $\tau$ up to 2.5 times

$< \tau >$. The bankfull scenario also shows a trimodal distribution, with two of the peaks representing bins of data less than the mean value. By referring back to Figure 17, it is observed that the smallest of these shear stresses occurs along the river banks while the largest shear stresses occur in the middle of the channel due to higher flow velocities.

Histograms comparing the uniform and variable roughness scenarios for the two highest flow levels (65.29 & 113.2 $m^3/s$) are shown in Figure 23.

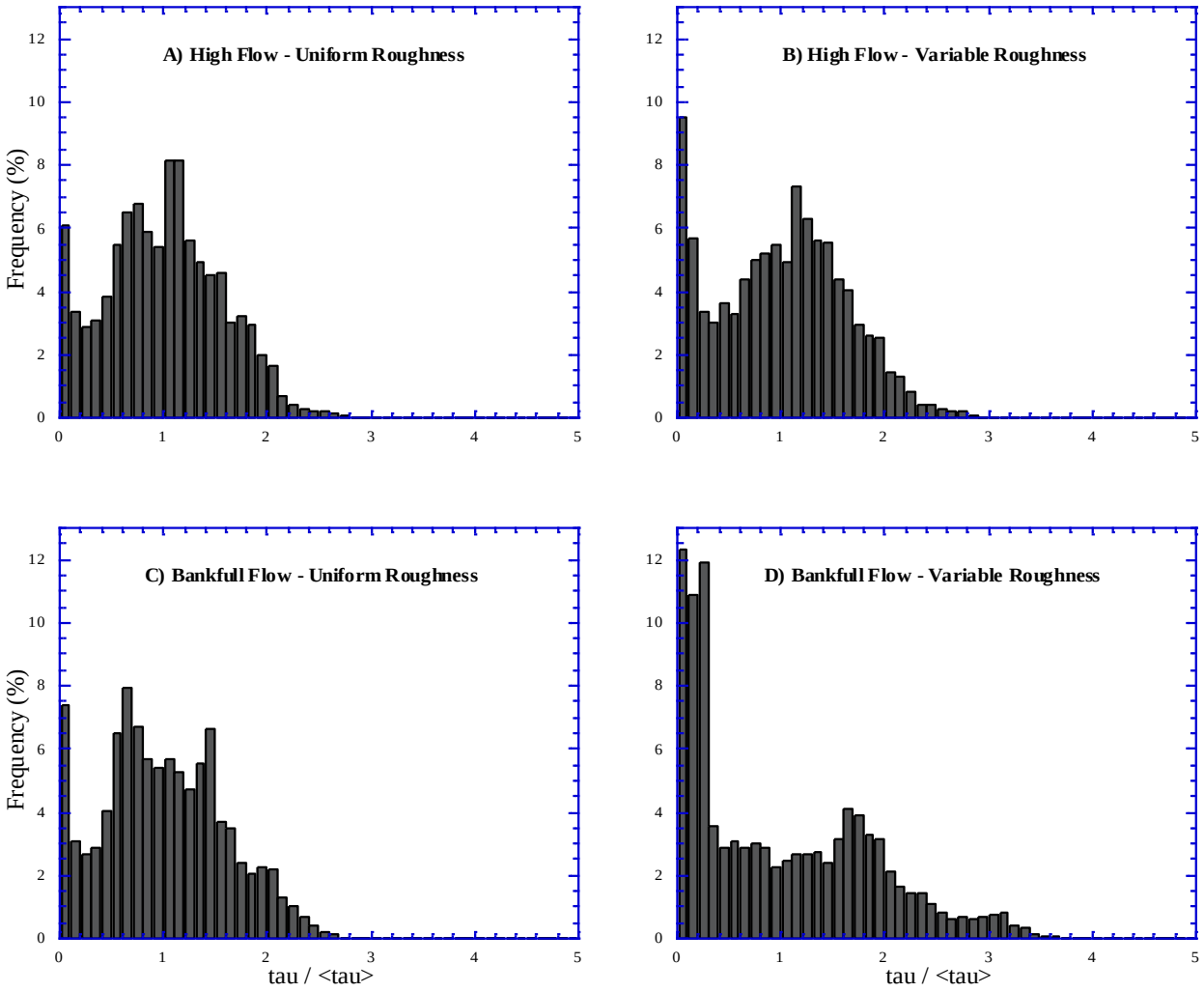


Figure 23. Histograms comparing the mean-normalized shear stress distributions of the two highest flow levels. The two left panels (A & C) show uniform roughness scenarios while the two right panels (B & D) show the variable roughness scenarios.

It can be observed that simulations where flow just begins to inundate the large northern bar, also incorporating the existence of riparian vegetation, have similar shear stress distributions as their uniform roughness counterparts. However, once the flow covers the majority of the bar, the distribution dramatically changes. Ranges in $\tau$ for the bankfull scenario increase to nearly 3.5 times $< \tau >$, but have a much larger frequency of low magnitude shear stresses. As discussed in the previous section and can be seen in Figures 19 and 20, the presence of vegetation on the large bar causes increased drag forces on the flow, drastically decreasing velocities and shear stresses over the bar. These drag forces divert water into the main channel, increasing flow velocities and shear stresses. This is why we see an increase in large magnitude shear stresses between the bankfull and high flow simulations with riparian vegetation.

Although the mean-normalized distributions of $\tau$ tend towards a behavior of increased symmetry with increased discharge for the uniform roughness scenarios, the absolute values of $\tau$ vary greatly. The mean, median, and range of $\tau$ values all increase with increased discharge. Estimates of reach average shear stress were calculated using equation 7:

$$\tau = \rho g S \bar{h} \quad , \tag{7}$$

where $\bar{h}$ is the average of simulated flow depths and S is the channel slope. At the study area, the reach average slope is approximately 0.001 m/m. Results summarized in Table 6 show that the calculated reach average $\tau$ is larger than the model output average $\tau$ for the two lowest flow levels, but smaller for the two larger flow levels in both the uniform and variable roughness scenarios. This indicates that at smaller discharges (5.76 and 14.90 $m^3/s$), the average channel slope is greater than the friction slope, whereas with larger flow levels (65.29 and 113.20 $m^3/s$), this relationship is reversed and the friction slope is larger than the channel slope.

Table 6. Summary of shear stress distribution values including fraction of bankfull flow, statistics of shear stress distributions, percent greater/less than mean values, mean depth, and mean shear stress using calculated reach average and model output methods.

| Roughness / Flow Level | $Q_i$ ($m^3/s$) | $\frac{Q_i}{Q_{bf}}$ | $\tau_{mean}$ ($N/m^2$) | $\tau_{median}$ ($N/m^2$) | $\tau_{max}$ ($N/m^2$) | $\tau > \tau_{mean}$ (%) | $\tau < \tau_{mean}$ (%) | $\bar{h}$ (m) | $\tau_{mean\text{ - reach}}$ ($N/m^2$) | $\tau_{mean\text{-model}}$ ($N/m^2$) |
|---|---|---|---|---|---|---|---|---|---|---|
| Uniform Roughness | | | | | | | | | | |
| Low Flow | 5.76 | 0.05 | 1.94 | 1.42 | 16.68 | 38.1 | 61.9 | 0.39 | 3.84 | 1.94 |
| Medium Flow | 14.9 | 0.13 | 2.71 | 2.57 | 12.02 | 46.8 | 53.2 | 0.48 | 4.73 | 2.71 |
| High Flow | 65.29 | 0.58 | 9.47 | 9.59 | 27.48 | 50.8 | 49.2 | 0.93 | 9.08 | 9.47 |
| Bankfull Flow | 113.2 | 1.00 | 13.09 | 12.55 | 37.82 | 47.7 | 52.3 | 1.05 | 10.35 | 13.09 |
| Variable Roughness | | | | | | | | | | |
| High Flow | 65.29 | 0.58 | 12.56 | 12.92 | 38.02 | 51.5 | 48.5 | 1.02 | 9.96 | 12.56 |
| Bankfull Flow | 113.2 | 1.00 | 16.23 | 12.68 | 62.77 | 44.4 | 55.6 | 1.15 | 11.31 | 16.23 |

## 4.3 Sediment Transport Rates

The model-simulated bed shear stress was used with a sediment transport relation to quantify transport rates during streamflows ranging between 5.76 $m^3/s$ (0.05 $Q_{bf}$) to 113.20 $m^3/s$ ($Q_{bf}$). To obtain estimates of the total sediment flux (sum of bed and suspended load) in the study reach, FaSTMECH utilizes the Engelund-Hansen sediment transport equation (Engelund and Hansen, 1967):

$$\Phi = \frac{0.1}{f}\tau^{*5/2} \tag{8}$$

where $\Phi$ is a non-dimensional sediment discharge, f represents a friction factor, and $\tau^*$ is the dimensionless shear stress. The non-dimensional sediment flux ($\Phi$) is defined as:

$$\Phi = \frac{q_T}{\sqrt{(s-1)gD^3}} \quad , \tag{9}$$

where $q_T = {Q_T}/{B}$ , $Q_T$ is the total sediment discharge (= $Q_B$ + $Q_S$), $Q_B$ is the discharge of bed load, $Q_S$ is the discharge of suspended load, B is the water surface width, s is the specific gravity of sediment, and D is the particle diameter size (m). The friction factor (f) is further defined as:

$$f = \frac{2g\bar{h}S}{\bar{U}^2} \quad , \tag{10}$$

where $\bar{h}$ is the mean depth of flow, S is the channel slope, and $\bar{U}$ is the mean velocity. The dimensionless form of bed shear stress is defined as:

$$\tau^* = \frac{\tau_o}{(\rho_s - \rho)gD} \quad , \tag{11}$$

where $\tau_o$ is the bed shear stress, $\rho_s$ is the density of sediment, and $\rho$ is the density of water. The bed shear stress is calculated according to:

$$\tau_o = \rho C_d (u^2 + v^2) \quad , \tag{12}$$

where u and v are the vertically averaged streamwise and cross-stream velocities, respectively.

FaSTMECH outputs values for shear stress as a total bed shear stress ($\tau_o$). In sandbed channels where bedforms are present, such as the study site of interest, total bed shear stress can be partitioned into two components (McLean, 1992): the shear stress acting on the sediment particles ($\tau_s$), also referred to as the grain shear stress, and the shear stress acting on the bed forms ($\tau_f$). Only the grain shear stress is responsible for the movement of sediment, thus a correction proposed by Smith and McLean (1977) is used to calculate the proportion of total bed shear stress associated with grain shear stress:

$$\frac{\tau_s}{\tau_o} = \frac{1}{1 + \left( \frac{C_d}{2k^2} \frac{\Delta}{\lambda} \left( ln\left( \frac{0.368\Delta}{z_0} \right) \right)^2 \right)} \quad , \tag{13}$$

where $\tau_s$ is the grain shear stress, k is von Karman's constant and typically has a value of 0.4, $\Delta$ is the wave height of the bedform, $\lambda$ is the wavelength of the bedform, $z_o$ is the roughness height and is defined as $z_o=0.12\ d_{84}$, where the $d_{84}$ is the $84^{th}$ percentile particle diameter.

The sediment grain size at the study site was set to 2.7 mm, representative of coarse sand and very fine gravel particles, and was assumed to be uniform throughout the reach. In order to obtain the most accurate estimates of sediment transport rates, assumptions for both dune wavelength ($\lambda$) and dune height ($\Delta$), representing sand bedforms, were made and input into the FaSTMECH model. Estimates of these two variables were obtained by assuming a bed-form steepness of 0.04 and referencing Figure 5 from (van Rijn, 1984b). Dune wavelength was set to a value of 7.5 m and dune height set to a value of 0.30 m. After calculations, it was determined that $\tau_s$ represents 65.14% of the total bed shear stress when using a $d_{84}$ of 9 mm.

In the Engelund-Hansen transport equation, there is no use of a critical shear stress ($\tau_c$), which is commonly used in many other transport equations denoting the shear stress required for incipient motion. Because of this, the Enguland-Hansen equation allows for areas with extremely low shear stress magnitudes to transport sediment. In order to best see the effects of riparian vegetation on sediment transport rates in this low sloping river, simulations were run for all four flow levels for both the uniform and spatially variable Manning's n, plus a single simulation representing a larger flood (169.8 $m^3/s$) with uniform roughness. This flow, according to Figure 8, approximately represents a 4-year flood event. Table 7 summarizes the results of the sediment transport simulations.

Table 7. Modeled sediment transport rates for varying flow levels and varying roughness scenarios. The column labeled % wet cells shows percent of cells that are wet (have a noticeable depth of water) compared to the 57,246 total cells, and the column labeled % movement cells represents percentage of wet cells that experience sediment fluxes. The units of sediment flux are in metric tonnes /day.

| Roughness / Flow Level | $Q_i$ ($m^3/s$) | % Wet Cells | % Movement Cells | Sed. Flux ($m^2/s$) | Sed. Flux (mt/day) |
|---|---|---|---|---|---|
| Uniform Roughness | | | | | |
| Low Flow | 5.76 | 20.76 | 20.14 | 0.00 | 1.4 |
| Medium Flow | 14.9 | 26.78 | 33.13 | 0.03 | 20.4 |
| High Flow | 65.29 | 35.63 | 87.61 | 1.16 | 714.2 |
| Bankfull Flow | 113.2 | 43.89 | 89.22 | 3.48 | 2,140.4 |
| 4-yr Flood | 169.8 | 51.57 | 87.05 | 8.56 | 5,263.2 |
| Variable Roughness | | | | | |
| Low Flow | 5.76 | 19.08 | 26.82 | 0.05 | 30.5 |
| Medium Flow | 14.9 | 25.59 | 61.19 | 0.21 | 128.1 |
| High Flow | 65.29 | 35.69 | 84.12 | 4.20 | 2,585.3 |
| Bankfull Flow | 113.2 | 47.96 | 76.88 | 15.87 | 9,756.2 |

Table 7 shows that as the discharge increases, a higher percentage of total nodes are considered "wet" due to higher flow levels and increased inundation in the lateral direction. Alternatively, the percentage of wet nodes that experience sediment transport decreases from the high flow level to the bankfull flow in the variable roughness scenario. This occurs because the bankfull discharge flows over an increased portion of the study site, encompassing the large majority of the large sand bar on the northern bank. However, because of the effect of simulated vegetation on the bar, the shear stress on the bar drastically decreases due to much slower flow velocities and the squared relationship between velocity and bed shear stress as shown in equation 12. Table 7 also shows that the study area experiences much greater sediment transport rates when riparian vegetation exists. In fact, there is approximately an order of magnitude difference between the sediment flux rates comparing similar flow levels with different roughness

scenarios. The large differences in sediment flux are illustrated in Figure 24, showing modeled sediment fluxes from FaSTMECH, fit with first-order power regression models.

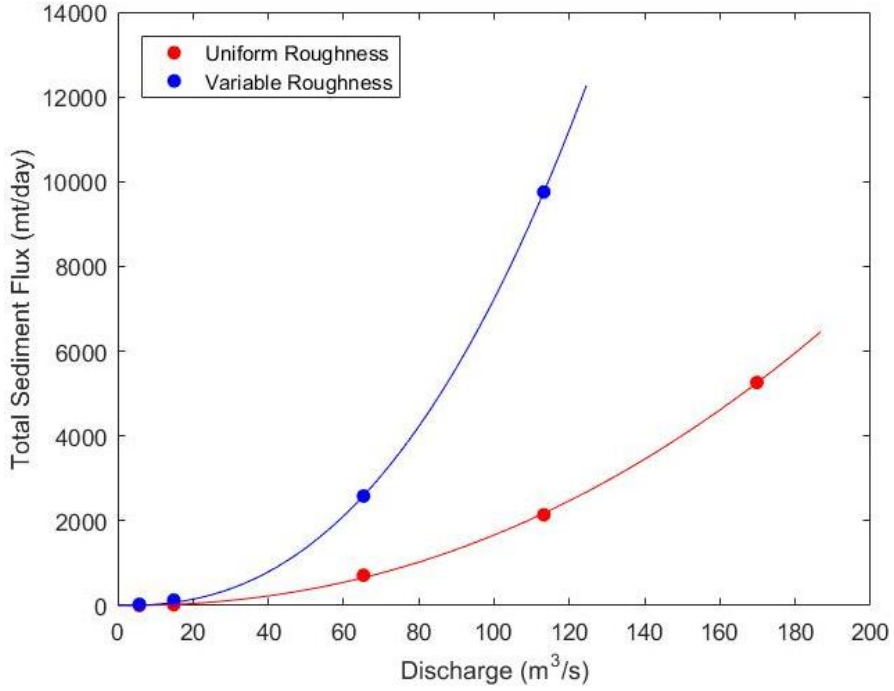


Figure 24. Differences in sediment transport fluxes for the chosen uniform and spatially variable roughness scenarios in metric tonnes/day.

The fitted regression between sediment flux ($Q_{sed}$) and discharge (Q) for the uniform roughness scenario is represented by equation 14 and the fitted regression for the spatially variable roughness scenario is represented by equation 15.

$$Q_{sed} = 0.076 * Q^{2.17} \tag{14}$$

$$Q_{sed} = 0.11 * Q^{2.41} \tag{152}$$

The parameters of these equations show us that the sediment fluxes for the variable roughness scenario exhibit a higher dependence on discharge than the uniform roughness scenario. This relationship makes intuitive sense because the Engelund-Hansen transport equations are dependent on $\tau^*$ raised to a power of 2.5, which increases not only with higher

discharge, but also with vegetated banks. When the large sand bar and river banks have higher roughness values, as is the case with the variable roughness scenario, a larger portion of the total flow is forced through the main (active) channel, causing both the depth and the velocity to increase.

Following the methods outlined in Li et al., (2015), it is estimated that there is significant sediment suspension during bankfull flows. Their study reported a curve developed from a multitude of data sets that denotes the start of "mostly suspension" load in gravel bed rivers during bankfull flows. This equation takes the form:

$$\tau^*_{bf\_threshold} = 1223\left(D^{*-1.00}\right)S^{0.534} \quad , \tag{16}$$

where $\tau^*_{bf}$ represents the bankfull dimensionless shear stress and D* is the dimensionless grain size, defined as follows.

$$D^* = \frac{(Rg)^{1/3}}{\nu^{2/3}}\, D \quad , \tag{17}$$

where R is the submerged specific gravity of quartz (1.65) and $\nu$ is the kinematic viscosity of water. Equation 18 was used to calculate a representative dimensionless shear stress during bankfull flows:

$$\tau^*_{bf} = \frac{\overline{h_{bf}}S}{RD} \quad , \tag{18}$$

where $\overline{h_{bf}}$is the average bankfull depth of the river. Using a calculated average bankfull depth of 2.66 m for the study site, values of 68.3, 0.45, and 0.60 were calculated for D*, $\tau^*_{bf\_threshold}$, and $\tau^*_{bf}$, respectively. Because $\tau^*_{bf} > \tau^*_{bf\_threshold}$, it was determined that at bankfull flows, most of the sediment in the reach is transported in suspension.

To assess the validity of the modeled transport rates, the calculated sediment fluxes output from the FaSTMECH model were then compared to sediment measurements reported on the South Platte River near Kersey, Colorado. Figure 25 shows modeled total sediment fluxes plotted with suspended sediment flux data from USGS gauge No. 0675400, approximately 20 km downstream (north) of the study site.

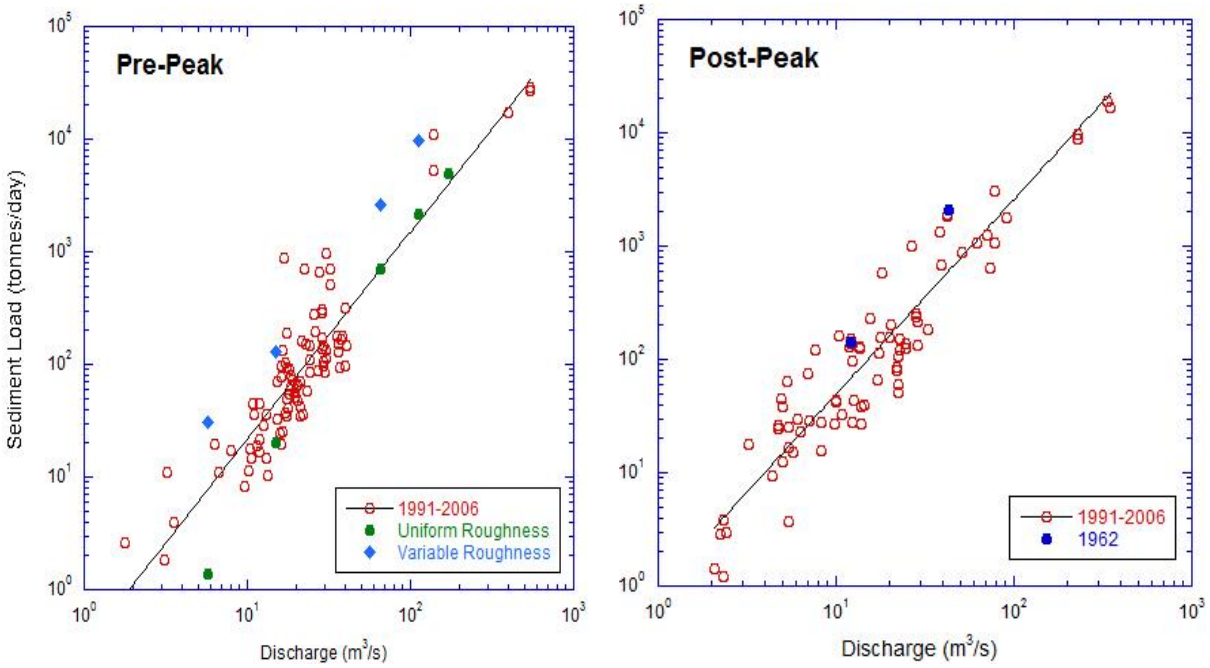


Figure 25. Plots of suspended sediment data (in metric tonnes per day) vs. discharge reported at USGS stream gauge No. 06754000 near Kersey, Colorado. The plot on the left shows measurements taken before the annual peak discharge and the plot on the right shows measurements taken after the annual peak discharge. The green and blue data points on the left plot show total sediment load (bed load and suspended load) of the model simulation outputs for both uniform and variable roughness scenarios.

FaSTMECH model output data were added to the pre-peak plot as they occurred during the testing period before the bankfull flow. It can clearly be seen that for model runs with variable roughness modeled sediment loads are higher than the values measured by the USGS. However, it is important to note that the data points from the FaSTMECH output are total load

(summation of bed load and suspended load) while the USGS only measures suspended load. By comparison, we see that the majority of the sediment being transported in the river, especially during times of high flow, is indeed in suspension. Furthermore, the loads carried by a given flow (Q) align closely with those presented by Pitlick, (2007), which represent transport of silt, clay, and sand in the Colorado River, further supporting our model results. The fitted regression models for pre-peak flows and post-peak flows are shown in equations 19 and 20, respectively:

$$Q_{sed} = 0.309 * Q^{1.85} \quad (19)$$

$$Q_{sed} = 0.937 * Q^{1.72} \quad (20)$$

These equations have lower exponents than the best fit relations derived from the model (equations 14 and 15). This conceptually makes sense as the data reported at the USGS gauge only represents suspended sediment while the model outputs total sediment which includes bed load, thus making the overall sediment load larger.

## 4.4 Sensitivity Analysis

A description for how the representative variable vegetation roughness values were chosen was given earlier in the methods section. Many assumptions had to be made in order to come up with these roughness values and thus a sensitivity analysis was conducted to see how the sediment transport rates would differ with varying vegetation roughness values. Following the same procedure outlined in Arcement and Schneider, (1989), values for Manning's n representative of willow that are semi-densely populated, oriented normally to flow, and averaging in height between 1-2 meters were decreased by as much as 50% and increased by as

much as 100%. Equation 3 was used to convert Manning's n values into a model friendly vegetation roughness for each discharge level for both the uniform and variable roughness scenarios. The model output results for the variable roughness scenario only are shown in Table 10.

Table 8. Calculated vegetation roughness values based on decreasing Manning's n-values by as much as 50% and increasing them by as much as 100%. Calculated sediment fluxes are shown in metric tonnes per day for each discharge value, representing only the variable roughness simulations.

| | | | Calculated Sediment Transport (tonnes/day) | | | |
|---|---|---|---|---|---|---|
| Manning's n | (+/-) % | $C_{d\text{-}veg}$ | 5.76 ($m^3/s$) | 14.9 ($m^3/s$) | 65.29 ($m^3/s$) | 113.2 ($m^3/s$) |
| 0.05 | - 50% | 0.033 | 8.88 | 82.10 | 2605.12 | 9442.50 |
| 0.1 | - | 0.133 | 7.48 | 73.79 | 2592.70 | 9761.20 |
| 0.15 | + 50% | 0.3 | 6.35 | 67.13 | 2627.44 | 10297.46 |
| 0.2 | +100 % | 0.533 | 5.64 | 62.92 | 2671.13 | 10790.41 |

Although the value for Manning's n varies from -50% to as much as +100% and the range in $C_d$ values is even greater, the sediment transport rates are nearly unaffected for small discharges. It isn't until the bankfull flow (113.20 $m^3/s$) that we see significant differences in the sediment flux (nearly 1,350 metric tonnes/day). This is due to the fact that the Engelund-Hansen transport equation depends on $\tau^{*5/2}$. It can be seen that altering the vegetation drag coefficient for the high flow simulations results in a range of depths of only 0.031 m and a range in velocities of 0.014 m/s. However, when comparing the bankfull flow simulation, altering the vegetation drag coefficient from 0.033 to 0.533 results in a 2.1% increase in depth and a 9.3% decrease in velocity. This occurs because when the river experiences bankfull flows, almost the entirety of the large northern sand bar is inundated. However, when the vegetation roughness is low, there is less resistance on the flow of water, allowing for higher velocities over the large sand bar thus increasing the average velocity and having a larger effect on sediment fluxes.

Table 9. Effect of altering the values for non-dimensional vegetation roughness on mean depth and mean velocity within the study area during the high and bankfull discharge simulations.

| | High Flow (65.29 $m^3/s$) | | | | Bankfull Flow (113.2 $m^3/s$) | | | |
|---|---|---|---|---|---|---|---|---|
| | Cd=.033 | Cd=.133 | Cd=.30 | Cd=.533 | Cd=.033 | Cd=.133 | Cd=.30 | Cd=.533 |
| Mean Depth (m) | 1.004 | 1.015 | 1.026 | 1.035 | 1.144 | 1.153 | 1.159 | 1.168 |
| Mean Velocity (m/s) | 1.143 | 1.129 | 1.129 | 1.134 | 1.221 | 1.159 | 1.13 | 1.117 |

The effects of varying the drag coefficient are shown in Figure 26, which plots the model output data points of sediment flux vs. discharge with fitted power regression models for the variable roughness scenario with different vegetation roughness values. It can clearly be seen that there are very little differences in sediment transport rates during times of low to moderate flows, but as the discharge gets larger, the distributions begin to separate more and more due to larger differences in velocity distributions.

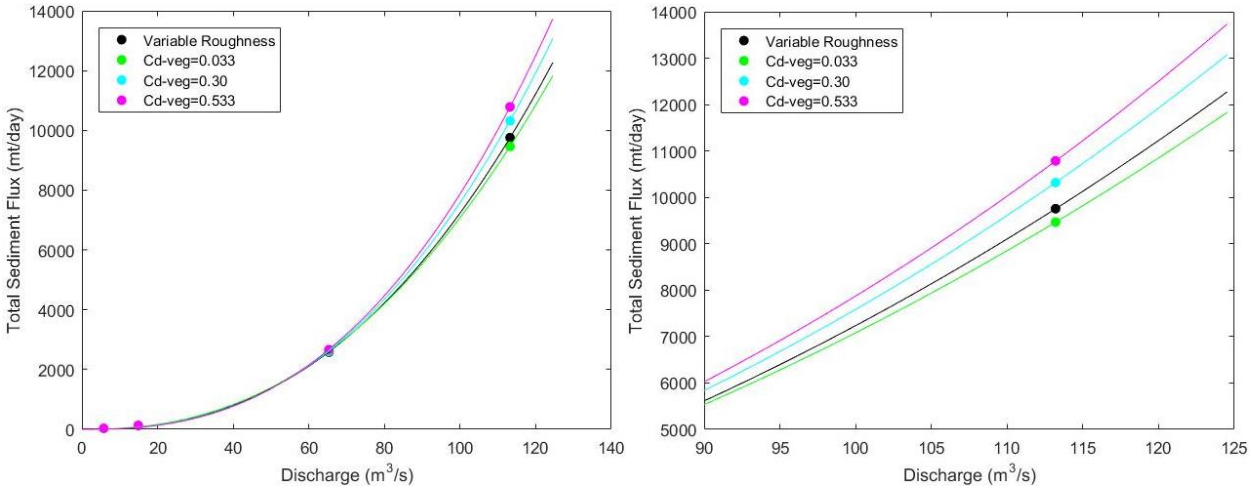


Figure 26. Plots of total sediment flux (in metric tonnes per day) for the different dimensionless vegetation drag coefficient values, all associated with the variable roughness simulations. The left panel shows the entire range of discharges while the right panel shows a zoomed in portion of the distributions, including discharge values more near bankfull flows. The distribution labeled "variable roughness" represents the base situation chosen to model throughout this study.

The equations below show the fitted power regression models for variable vegetation roughness scenarios of $C_{d\text{-}veg}$=0.033, 0.133 (base), 0.30, 0.533, respectively:

$$Q_{sed} = 0.148 * Q^{2.34} \quad (21)$$

$$Q_{sed} = 0.11 * Q^{2.41} \quad (22)$$

$$Q_{sed} = 0.082 * Q^{2.48} \quad (23)$$

$$Q_{sed} = 0.067 * Q^{2.54} \quad (24)$$

From this analysis, it is evident that altering the values of the non-dimensional vegetation drag coefficient only has significant impacts on sediment transport rates during discharges nearing bankfull flow. This is important firstly because it is known that a significant portion of the large sand bar, which highly controls sediment transport rates, is only covered by flowing water during discharges very near bankfull flow. Additionally, this is important because it tells us that by drastically changing the value of $C_{d\text{-}veg}$, there are major differences in sediment transport rates between vegetated and non-vegetated sand bars and river banks. However, when comparing multiple scenarios with riparian vegetation, alterations to $C_{d\text{-}veg}$, representing differences in vegetation density, height, orientation, leafy/leafless structure, age, rigidity, and vegetation type, only slightly affect sediment fluxes.

# 5 DISCUSSION

The results of this study confirm that the presence of riparian vegetation can have a large impact on sediment transport within the South Platte River. In fact, our findings show an almost order of magnitude increase in sediment flux within the main channel of the river for all flow levels. However, we have also shown how variations in vegetation type and structure, represented as a dimensionless drag coefficient, have very little effect on the overall sediment budget. This knowledge is very important and could be used in flood mitigation practices in regions characteristic of wide floodplains with low-sloping meandering rivers. The study site in this research was characteristic of bushy willow on the river banks, but had a large barren sand bar that became inundated during large flow events. Our study has shown that if vegetation becomes established on this bar, the majority of the river's flow would be directed into the main channel, leading to small depths and low velocities across the bar. This in turn means that there is much more sediment transport occurring in the main channel leading to more scour of the river bed and bank walls, causing large erosion rates.

From further analysis of the model results, we see that the sediment flux does not remain equal between cross-sections, indicating that either deposition/erosion is occurring. Calculated sediment flux rates sometimes vary as much as an order of magnitude between upstream and downstream cross-sections. This most likely is due to channel characteristics at the different cross-sections. During high flows, we see higher sediment fluxes at XS-5 where the river is relatively narrow and the flow velocities in the main channel are highest. We have previously shown that most of this transport is in suspension, but once the flow reaches XS-2 where the channel becomes wider and the velocities decrease, some of the sediment is dropped out of suspension and moves as bed load. Table 10 summarizes some of these results.

Table 10. Summary of reported sediment flux loads, in metric tonnes per day, for a few chosen cross-sections. These cross-sections were chosen due to their perpendicular angle with respect to the river flow direction and to gather a range of data in the middle of the reach and the near the upstream and downstream boundaries.

| Roughness / Flow Level | Cross-Sectional Sediment Flux Rates (tonnes/day) | | | | |
|---|---|---|---|---|---|
| | XS-2 | XS-4 | XS-5 | XS-12 | XS-13 |
| Uniform Roughness | | | | | |
| Low Flow | 3.97 | 17.19 | 1.76 | 26.00 | 54.28 |
| Medium Flow | 3.21 | 1.27 | 1.18 | 44.78 | 51.60 |
| High Flow | 447.83 | 735.73 | 735.99 | 464.69 | 262.03 |
| Bankfull Flow | 2010.67 | 3488.58 | 3247.28 | 707.19 | 577.80 |
| Variable Roughness | | | | | |
| High Flow | 2008.36 | 2578.07 | 2680.24 | 1595.99 | 949.23 |
| Bankfull Flow | 8371.56 | 13592.21 | 15357.15 | 3081.24 | 2063.23 |

This study focused on quantifying the effect of vegetation on instantaneous transport rates, however, further research could be conducted using FaSTMECH's time-dependent simulation capabilities to study the changes of the bed topography over time. Knowing that the sediment flux varies between cross-sections within the river is important because it tells us that erosion/deposition is occurring. This will change the bed morphology within the river over time and could lead to bank erosion and channel widening. This has potential to have major impacts on habitat area for freshwater fish and other riverine species.

By making the assumption that model inputs remain constant over time, we were able to extrapolate model results to come up with estimates for total sediment transported within the study area over a day. These results (Table 7) align closely with many other studies conducted in Idaho (Barton et al., 2005; Berenbrock, 2008), Colorado (Pitlick, 2007; Segura and Pitlick, 2015), and a combination of states along the Rocky Mountains (Mueller and Pitlick, 2013; Pitlick et al., 2008). However, the results corresponding to the spatially variable roughness scenarios were dependent on estimates for a dimensionless drag coefficient representative of the willow found in the field. Although using the USGS "Guide for Selecting Manning's Roughness

Coefficients for Natural Channels and Flood Plains" is a fairly crude method for determining lumped surface roughness based on bed topography characteristics and flow obstructions, the final results match those of other studies. The depth averaged non-dimensional roughness coefficient representative of the middle-aged leafy willow found at the study area was set to a value of 0.133, which is similar to values reported in Fischenich and Dudley, (2000) and Hui et al., (2010). Our choice of $C_{d\text{-}veg}$ is further validated by comparing our model results of sediment flux with field measurements conducted by the USGS only 20 km downstream of the study site (Figure 25).

Although FaSTMECH was able to accurately produce estimates of sediment transport, supported by other data sets across the Rocky Mountains, the model is unable to incorporate more complex plant morphology. The largest flow modeled in this study was the bankfull flow, which inundates the large northern sand bar at the study site and just barely reaches portions of the flood plain. This means that only the base of the vegetation is covered by flowing water and thus a representative vegetation surface roughness is sufficient. However, during larger flood events such as the historical flood of 2013 when the floodplains experienced flow depths of several feet, the model is unable to capture the effect of vegetation on flow throughout the vertical water column, the changes in drag associated with the rigid/flexible behavior of vegetation, or the height and orientation to flow. This means that in order to most accurately estimate sediment fluxes during very large flood events, a different approach to modeling the direct effects of vegetation on flow dynamics and sediment transport should be considered.

The FaSTMECH model uses the Engelund-Hansen (E-H) equation (equations 8-12) to calculate the total sediment load (bed load and suspended load) throughout the simulation. The Engelund-Hansen equation (1967) is one of the most widely used transport relationships still

used today because of its theoretical basis. As shown throughout this study, the model results of sediment flux align closely with reported values from other studies. It is interesting to note however, that the Engelund-Hansen transport equation, unlike many other transport models (the Meyer-Peter Muller, Wilcock and Crowe, Wilcock and Kenworthy, and the Kuhnle et al.), does not utilize a critical shear stress ($\tau_c$). The $\tau_c$ is defined as the shear stress required for incipient motion to occur. Because the E-H equation does not utilize such a variable, transport could theoretically occur under any circumstances. Knowing that this is not always physically reasonable, questions arise to the validity of the calculated results. However, we see from Figure 23 that vegetation causes a higher frequency of low shear stress values when compared to their uniform roughness counterparts. The results outlined in Table 8 show the percent of cells in the grid that experience movement decreases for these scenarios with a larger percentage of low shear stresses. This leads us to believe that although there is no threshold value of shear stress required for movement of sediment particles, the underlying physics relationships in the E-H equation prevents unrealistic calculations of transport to a high degree.

# 6 CONCLUSIONS

This study utilized a two-dimensional flow model, FaSTMECH, in combination with field survey data, to quantify the effects of riparian vegetation on flow dynamics and sediment transport rates in a reach of the South Platte River, just downstream of Fort Lupton. A dimensionless drag coefficient representative of the bushy willow found on the river banks was input into the model. Simulations were run at varying discharge levels (0.05 $Q_{bf}$ to $Q_{bf}$) with both uniform and spatially variable roughness to study the effects of vegetation.

Spatial distributions of shear stress represent a river's ability to transport sediment and is largely affected by changes in bank roughness caused by the presence of vegetation. It can be seen that the distribution of mean-normalized shear stresses for the uniform roughness scenarios tend towards normality with increased flow levels. The changes in flow level result in a gradual transition in the median and interquartile range of shear stress, with most of this transition related to changes in velocity in the main channel, rather than over the large sand bar. However, the distributions representing the spatially variable roughness scenarios characteristic of vegetation presence show a large increase in low magnitude shear stress values over the large bar. Vegetation on the river banks and large bars causes increases in flow resistance, diverting a larger portion of the flow into the main channel. In this scenario, we see an order of magnitude decrease of shear stress over the river banks and large increases within the main channel where flow velocities are highest. It can be seen that the variable roughness scenarios are characterized by larger magnitude shear stresses when compared to their uniform roughness counterpart simulations. Although the median values are similar, there exists a much larger proportion of shear stresses with higher magnitudes for the variable roughness simulations. These differences

show that the growth of riparian vegetation has large effects on the flow over the large sand bar as well as the main channel.

Sediment transport rates are largely controlled by the distribution of large shear stresses caused by vegetation (increased bank roughness). Model results show a clear increase in sediment fluxes at varying discharges with the presence of vegetation along river banks. Transport rates increase by an order of magnitude with the presence of vegetation at all flow levels, however, the differences vary the greatest at bankfull flow. Power regression models were fit to the relationships between sediment fluxes and discharge with an exponent of 2.171 for the uniform roughness scenario and an exponent of 2.409 for the variable roughness scenario. We see that these results align closely with field measurements conducted by the USGS only 20 km downstream of our study site, validating our model results.

A sensitivity analysis was conducted in order to study how changes in vegetation characteristics affect sediment transport rates. Initially, a crude method was used in order to come up with a dimensionless drag coefficient representative of the willow found at the study site. We altered $C_d$ by as much as +/- 400%, representing differences in vegetation density, height, orientation, leafy/leafless structure, age, rigidity, and vegetation type. We find that although there is a relationship between sediment fluxes and changes in $C_d$, there only exists a 14% increase in sediment transport at $Q_{bf}$ between the two exterior limits of $C_d$. It is evident that there is a strong impact on riparian vegetation on both flow dynamics and sediment transport rates. However, we also find that these changes are not unique to the vegetation found at the study site and that we would find similar results if any changes in the vegetation structure were to take place.

# References

Andrews, E.D., 1980. Effective and bankfull discharges of streams in the Yampa River basin, Colorado and Wyoming. J. Hydrol. 46, 311–330. doi:10.1016/0022-1694(80)90084-0

Arcement Jr., G.J., Schneider, V.R., 1989. Guide for Selecting Manning's Roughness Coefficients for Natural Channels and Flood Plains (Water-Supply Paper No. 2339). U.S. Geological Survey.

Barton, G.J., McDonald, R.R., Nelson, J.M., Dinehart, R.L., 2005. Simulation of flow and sediment mobility using a multidimensional flow model for the White Sturgeon critical-habitat reach, Kootenai River near Bonners Ferry, Idaho (USGS Numbered Series No. 2005-5230), Scientific Investigations Report.

Berenbrock, C., 2008. Simulation of flow, sediment transport, and sediment mobility of the lower Coeur d'Alene River, Idaho. U.S. Geological Survey, Reston, Va.

Castro, J.M., Jackson, P.L., 2001. Bankfull Discharge Recurrence Intervals and Regional Hydraulic Geometry Relationships: Patterns in the Pacific Northwest, Usa1. JAWRA J. Am. Water Resour. Assoc. 37, 1249–1262. doi:10.1111/j.1752-1688.2001.tb03636.x

Chang, T.-H., Chen, S., Huang, S.-T., 2011. Shelter effect evaluation of the willow works bank protection method: a case study for Beinan River Reach 2009 Typhoon Morakot event. Paddy Water Environ. 11, 15–33. doi:10.1007/s10333-011-0288-9

Clayton, J.A., Pitlick, J., 2007. Spatial and temporal variations in bed load transport intensity in a gravel bed river bend. Water Resour. Res. 43, W02426. doi:10.1029/2006WR005253

Cooper, D.J., Dickens, J., Hobbs, N.T., Christensen, L., Landrum, L., 2006. Hydrologic, geomorphic and climatic processes controlling willow establishment in a montane ecosystem. Hydrol. Process. 20, 1845–1864. doi:10.1002/hyp.5965

Cronin, G., Mccutchan, J.H., Pitlick, J., Lewis, W.M., 2007. Use of Shields stress to reconstruct and forecast changes in river metabolism. Freshw. Biol. 52, 1587–1601. doi:10.1111/j.1365-2427.2007.01790.x

Dennehy, K.F., Litke, D.W., Tate, C.M., Heiny, J.S., 1993. South Platte River Basin - Colorado, Nebraska, and Wyoming. JAWRA J. Am. Water Resour. Assoc. 29, 647–683. doi:10.1111/j.1752-1688.1993.tb03231.x

Dunne, T., Leopold, L.B., 1978. Water in Environmental Planning. W. H. Freeman and Co., San Francisco, California.

Dury, G.H., J. R. Hails, H. B. Robbie, 1963. Bankfull discharge and the magnitude frequency series. Aust. J. Sci. 26, 123–124.

Engelund, F., Hansen, E., 1967. A monograph on sediment transport in alluvial streams. Teknisk Forlag, Copenhagen, Denmark.

Fathi-Maghadam, M., Kouwen, N., 1997. Nonrigid, Nonsubmerged, Vegetative Roughness on Floodplains. J. Hydraul. Eng. 123, 51–57. doi:10.1061/(ASCE)0733-9429(1997)123:1(51)

Fischenich, C., Dudley, S., 2000. Determining Drag Coefficients and Area for Vegetation, Ecosystem Management & Restoration Research Program SR 08. US Army Corps of Engineers.

Galema, A., 2009. Vegetation Resistance: Evaluation of Vegetation Resistance Descriptors for Flood Management. University of Twente, Enschede, Netherlands.

Hickin, E.J., 1968. Channel morphology, bankfull stage and bankfull discharge of streams near Sydney. Aust. J. Sci. 274–275.

Hui, E., Hu, X., Jiang, C., Ma, F., Zhu, Z., 2010. A study of drag coefficient related with vegetation based on the flume experiment. J. Hydrodyn. Ser B 22, 329–337. doi:10.1016/S1001-6058(09)60062-7

Huthoff, F., Augustijn, D.C.M., Hulscher, S.J.M.H., 2007. Analytical solution of the depth-averaged flow velocity in case of submerged rigid cylindrical vegetation. Water Resour. Res. 43, W06413. doi:10.1029/2006WR005625

Hu, Z., Stive, M., Zitman, T., Suzuki, T., 2012. DRAG COEFFICIENT OF VEGETATION IN FLOW MODELING. Coast. Eng. Proc. 1, 4.

Järvelä, J., 2002. Flow resistance of flexible and stiff vegetation: a flume study with natural plants. J. Hydrol. 269, 44–54. doi:10.1016/S0022-1694(02)00193-2

Julien, P.Y., 2002. River Mechanics. Cambridge University Press.

Kennedy, B.A., 1972. "Bankfull" Discharge and Meander Forms. Area 4, 209–212.

Kim, S.J., Stoesser, T., 2011. Closure modeling and direct simulation of vegetation drag in flow through emergent vegetation. Water Resour. Res. 47, W10511. doi:10.1029/2011WR010561

Legleiter, C.J., Kyriakidis, P.C., McDonald, R.R., Nelson, J.M., 2011. Effects of uncertain topographic input data on two-dimensional flow modeling in a gravel-bed river. Water Resour. Res. 47, W03518. doi:10.1029/2010WR009618

Leopold, L.B., 1994. A View of the River. Harvard University Press, Cambridge, Massachusetts.

Leopold, L.B., Wolman, M.G., Miller, J.P., 1964. Fluvial Processes in Geomorphology. W. H. Freeman and Co., San Francisco, California.

Li, C., Czapiga, M.J., Eke, E.C., Viparelli, E., Parker, G., 2015. Variable Shields number model for river bankfull geometry: bankfull shear velocity is viscosity-dependent but grain size-independent. J. Hydraul. Res. 53, 36–48. doi:10.1080/00221686.2014.939113

Lisle, T.E., Nelson, J.M., Pitlick, J., Madej, M.A., Barkett, B.L., 2000. Variability of bed mobility in natural, gravel-bed channels and adjustments to sediment load at local and reach scales. Water Resour. Res. 36, 3743–3755. doi:10.1029/2000WR900238

Logan, B.L., McDonald, R.R., Nelson, J.M., Kinzel, P.J., Barton, G.J., 2011. Use of multidimensional modeling to evaluate a channel restoration design for the Kootenai River, Idaho (USGS Numbered Series No. 2010-5213), Scientific Investigations Report. USGS, Reston, VA.

López, F., García, M., 1998. open-channel flow through simulated vegetation: Suspended sediment transport modeling. Water Resour. Res. 34, 2341–2352. doi:10.1029/98WR01922

McDonald, R., Nelson, J., Kinzel, P., Conaway, J., 2006. Modeling surface-water flow and sediment mobility with the Multi-Dimensional Surface-Water Modeling System (MD_SWMS) (USGS Numbered Series No. 2005-3078), Fact Sheet.

McLean, S.R., 1992. On the calculation of suspended load for noncohesive sediments. J. Geophys. Res. Oceans 97, 5759–5770. doi:10.1029/91JC02933

Molinas, A., Wu, B., 2001. Transport of sediment in large sand-bed rivers. J. Hydraul. Res. 39, 135–146. doi:10.1080/00221680109499814

Mueller, E.R., 2012. Landscape Controls on Sediment Supply and Stream Channel Morpho-Dynamics in the Northern Rocky Mountains (Dissertation). University of Colorado Boulder, Boulder, CO.

Murray, A.B., Paola, C., 2003. Modelling the effect of vegetation on channel pattern in bedload rivers. Earth Surf. Process. Landf. 28, 131–143. doi:10.1002/esp.428

Nelson, J.M., 1999. FaSTMECH Solver Manual (No. 2). U.S. Geological Survey, Lakewood, Colorado.

Nelson, J.M., Bennett, J.P., Wiele, S.M., 2003. Flow and sediment-transport modeling, in: Kondolph, G.M., Piegay, H. (Eds.), Tools in Fluvial Geomorphology. Wiley and Sons, Chichester, pp. 539–576.

Nelson, J.M., Smith, J.D., 1989. Flow in Meandering Channels with Natural Topography, in: Ikeda, S., Parker, G. (Eds.), River Meandering. American Geophysical Union, pp. 69–102.

Nelson, P.A., Dietrich, W.E., Venditti, J.G., 2010. Bed topography and the development of forced bed surface patches. J. Geophys. Res. Earth Surf. 115, F04024. doi:10.1029/2010JF001747

Petit, F., Pauquet, A., 1997. Bankfull Discharge Recurrence Interval in Gravel-bed Rivers. Earth Surf. Process. Landf. 22, 685–693. doi:10.1002/(SICI)1096-9837(199707)22:7<685::AID-ESP744>3.0.CO;2-J

Pitlick, J., 2007. Channel monitoring to evaluate geomorphic changes on the main stem of the Colorado River (Recovery Program Project No. 85A). University of Colorado, Geography Department, Boulder, CO.

Pitlick, J., Wilcock, P., 2001. Relations between streamflow, sediment transport, and aquatic habitat in regulated rivers. Geomorphic Process. Riverine Habitat, Water Science and Application 4, 185–198.

Rossi, L., 2014. Active bed in gravel-bed rivers: the case study of Fall River in Rocky Mountain National Park (Thesis). Universita Degli Studi Di Trento, Trento, Italy.

Segura, C., McCutchan, J.H., Lewis, W.M., Pitlick, J., 2011. The influence of channel bed disturbance on algal biomass in a Colorado mountain stream. Ecohydrology 4, 411–421. doi:10.1002/eco.142

Segura, C., Pitlick, J., 2015. Coupling fluvial-hydraulic models to predict gravel transport in spatially variable flows. J. Geophys. Res. Earth Surf. 120, 2014JF003302. doi:10.1002/2014JF003302

Shucksmith, J.D., Boxall, J.B., Guymer, I., 2010. Effects of emergent and submerged natural vegetation on longitudinal mixing in open channel flow. Water Resour. Res. 46, W04504. doi:10.1029/2008WR007657

South Platte River System in Colorado: Hydrology, Development, and Management Issues, 1990. . Colorado Water Resources Research Institute, Fort Collins, CO.

Tal, M., Gran, K., Murray, A.B., Paola, C., Hicks, D.M., 2004. Riparian Vegetation as a Primary Control on Channel Characteristics in Multi-thread Rivers. Riparian Veg. Fluv. Geomorphol. 8, 43–58. doi:10.1029/008WSA04

Tanaka, N., Yagisawa, J., 2010. Flow structures and sedimentation characteristics around clump-type vegetation. J. Hydro-Environ. Res. 4, 15–25. doi:10.1016/j.jher.2009.11.002

Tang, H., Tian, Z., Yan, J., Yuan, S., 2014. Determining drag coefficients and their application in modelling of turbulent flow with submerged vegetation. Adv. Water Resour. 69, 134–145. doi:10.1016/j.advwatres.2014.04.006

Van Rijn, L.C., 1984a. Sediment Transport, Part II: Suspended Load Transport. J. Hydraul. Eng. 110, 1613–1641. doi:10.1061/(ASCE)0733-9429(1984)110:11(1613)

Van Rijn, L.C., 1984b. Sediment Transport, Part III: Bed forms and Alluvial Roughness. J. Hydraul. Eng. 110, 1733–1754. doi:10.1061/(ASCE)0733-9429(1984)110:12(1733)

Van Rijn, L.C., 1984c. Sediment Transport, Part I: Bed Load Transport. J. Hydraul. Eng. 110, 1431–1456. doi:10.1061/(ASCE)0733-9429(1984)110:10(1431)

Williams, G.P., 1978. Bank-full discharge of rivers. Water Resour. Res. 14, 1141–1154. doi:10.1029/WR014i006p01141

Wu, W., Shields, F.D., Bennett, S.J., Wang, S.S.Y., 2005. A depth-averaged two-dimensional model for flow, sediment transport, and bed topography in curved channels with riparian vegetation. Water Resour. Res. 41, W03015. doi:10.1029/2004WR003730

# Appendix A: 1-Dimensional HEC-RAS Model Results

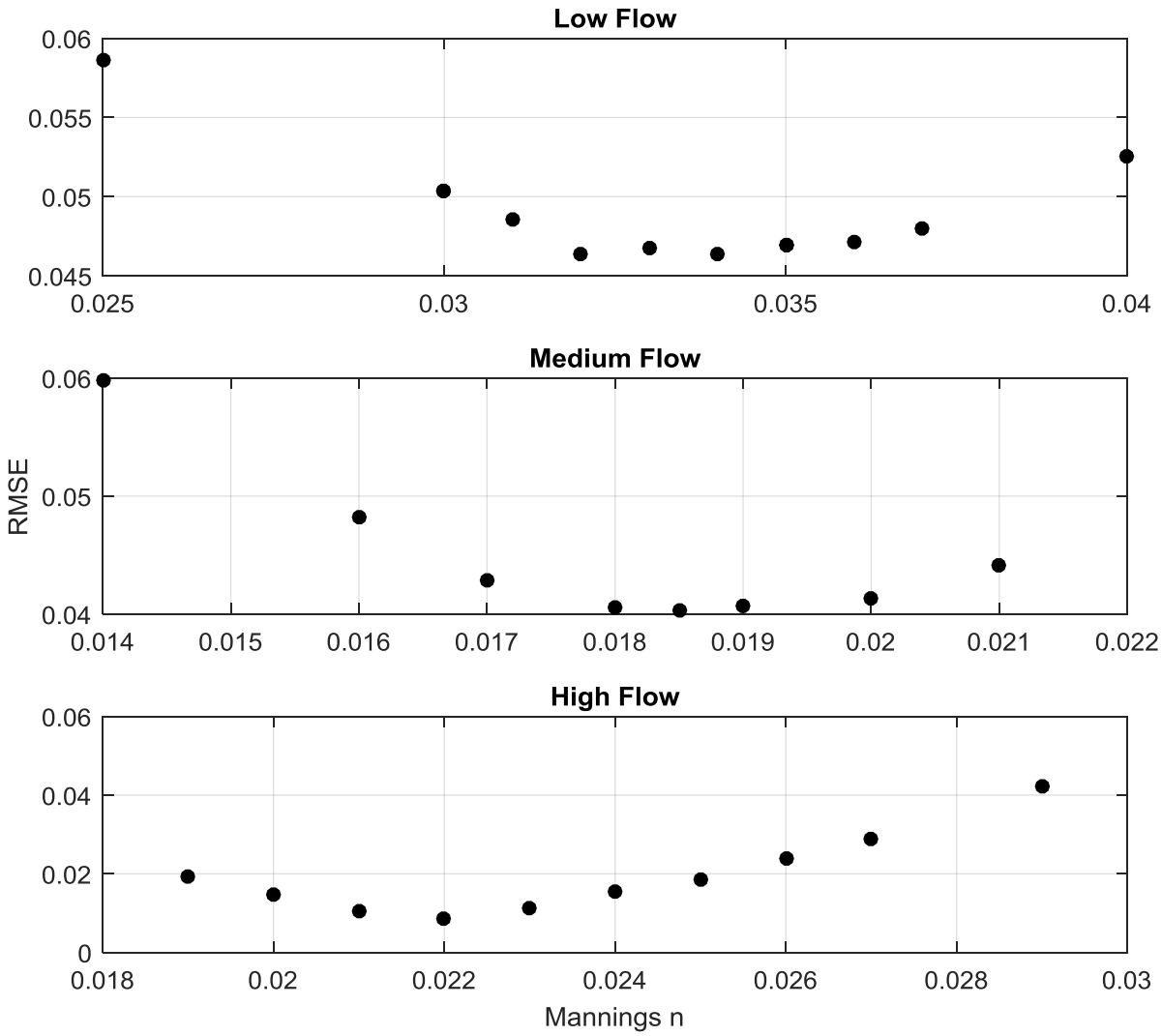


Figure 27. Calibration curves for the 3 preliminary simulations using a 1-D HEC-RAS model.

Because there were no measured WSEs for the bankfull flow level, it was assumed that the initial estimate of Manning's n found during the high flow scenario would be similar in magnitude to the bankfull discharge and thus were set to be equal.

Table 11. Summary of best fit Manning's n-values found using a preliminary 1-D HEC-RAS model.

| | Discharge ($m^3/s$) | Best Fit Manning's n | RMSE |
|---|---|---|---|
| Low Flow | 5.76 | 0.034 | 0.107 |
| Medium Flow | 14.90 | 0.0185 | 0.04 |
| High Flow | 65.29 | 0.022 | 0.009 |
| Bankfull Flow | 113.20 | 0.022 | - |

# Appendix B: Example Cross-Section Survey Data

Table 12. Example of surveyed cross-sectional data. This particular data represents XS-0.

| Distance (m) | Elevation (m) | Remarks |
|---|---|---|
| 0 | 1453.779 | BOT LEP |
| 1.896 | 1453.65 | |
| 3.943 | 1453.438 | |
| 7.362 | 1453.516 | |
| 10.283 | 1453.627 | |
| 13.089 | 1453.692 | |
| 15.932 | 1453.609 | TLB |
| 17.002 | 1452.435 | LEW - side channel |
| 18.473 | 1452.189 | |
| 21.48 | 1452.279 | |
| 24.114 | 1452.264 | |
| 27.103 | 1452.39 | |
| 30.07 | 1452.437 | REW - side channel |
| 33.312 | 1452.514 | |
| 36.491 | 1452.526 | |
| 39.567 | 1452.5 | |
| 42.844 | 1452.428 | LEW - side channel |
| 45.677 | 1452.342 | |
| 48.093 | 1452.275 | |
| 50.297 | 1451.957 | |
| 53.177 | 1451.799 | |
| 55.744 | 1451.797 | |
| 57.706 | 1451.843 | |
| 60.129 | 1451.887 | |
| 62.552 | 1451.905 | |
| 65.728 | 1451.926 | |
| 68.668 | 1451.894 | |
| 71.466 | 1451.69 | |
| 74.022 | 1451.458 | |
| 76.203 | 1451.27 | |
| 78.503 | 1451.536 | REC |
| 78.51 | 1451.549 | |
| 78.647 | 1452.436 | REW |
| 79.159 | 1453.695 | TRB |
| 80.384 | 1453.888 | |
| 83.026 | 1453.765 | |
| 85.76 | 1453.734 | BOT REP |
| 85.814 | 1453.883 | TOP REP |

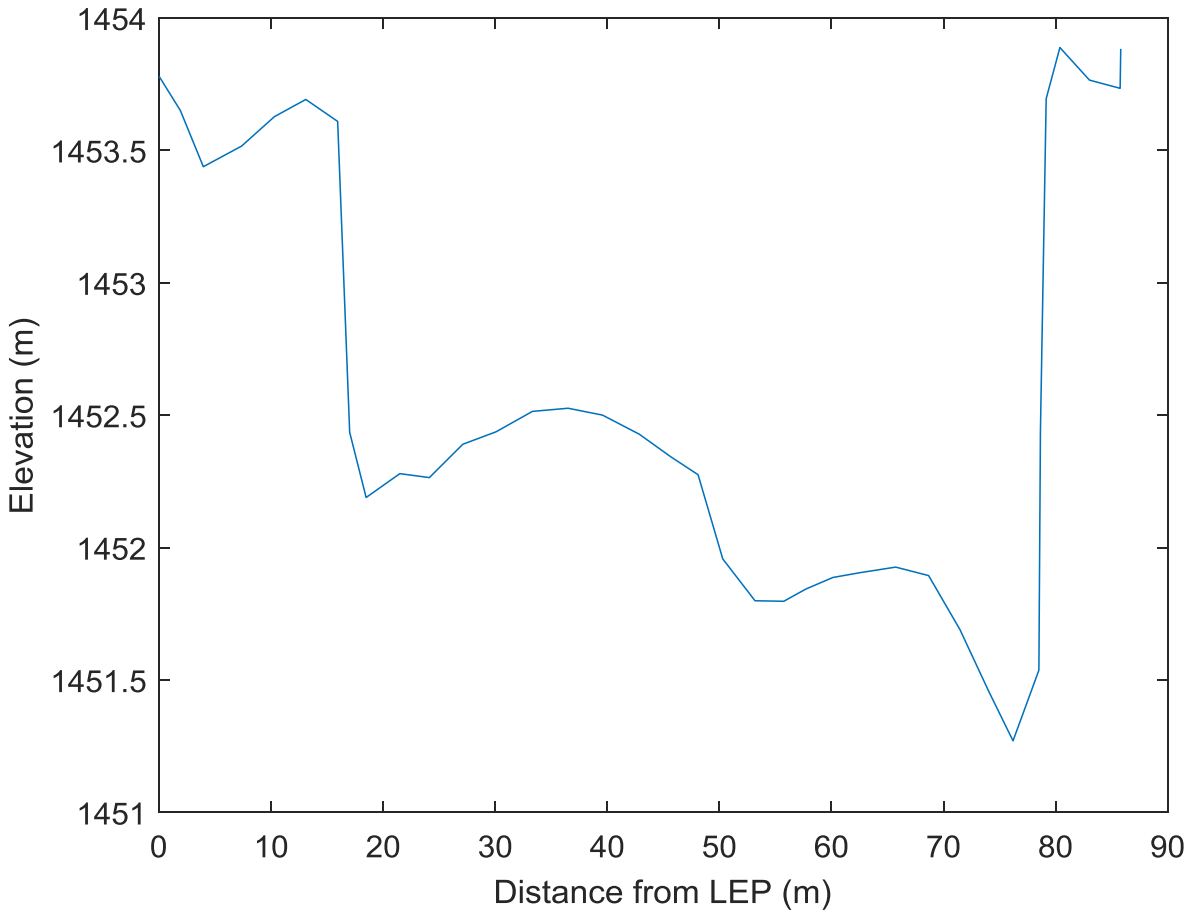


Figure 28. Example of a cross-sectional plot of river geometry. This particular plot represents XS-0.